Etching of hydrocarbon polymers with hyperthermal neutral beams
by James William Seale

A thesis submitted in partial fulfillment of the requirements for the degree of Master of Science in Chemical Engineering
Montana State University

Abstract:
The erosion of polymeric materials in atomic oxygen environments is important 1) as an aspect of materials degradation on spacecraft in low Earth orbit (LEO) and 2) in certain etch processes in the manufacture of microelectronic devices that involve the patterning of polymer films. In this work, directed beams of energetic neutral species have been tested as a means to achieve etching results that are superior to those obtained in plasma environments. In addition, molecular beam techniques have been employed to probe the mechanisms by which polymers erode. A laser detonation source, originally developed for ground-based testing of candidate spacecraft materials, was used to generate fast neutral species for these experiments. This source was coupled to a crossed molecular beams apparatus that has a rotatable mass spectrometer detector for analysis of volatile etch products.

The etching of a polyimide was conducted with a neutral beam of oxygen atoms created from precursor gases of N2O and O2 The results described in this thesis demonstrate the effect of incident energy and flux on the anisotropy and surface roughness of etched features. Etch anisotropy (undercutting) was minimized with the use of highly directional incident reactive species with high kinetic energies. Surface roughness was minimized with a higher reactive species flux on the surface and lower incident kinetic energies. The beam created from N2O etched more rapidly and yielded superior etch characteristics as compared to the beam created with O2.

Mechanistic studies were designed to investigate the material removal mechanism during steady-state etching. A effusive source of oxygen atoms was designed, built, and characterized. This source was used to direct a continuous stream of near-thermal oxygen atoms at a polymer surface, in order to approximate the steady-state oxidation conditions that would occur during plasma etching. The removal rate of a major reaction product, CO2, was significantly enhanced when pulsed beams of hyperthermal nonreactive species were directed at the continuously oxidized surface. Hyperthermal beams of N2 and Ar, with incident kinetic energies in the range 8 to 16 eV, apparently assisted in the release of CO2 through a collisional process that became important above 10 eV. The signal intensity of the volatile CO2 product increased exponentially with increasing incident energy. The large increase in CO2 removal rate through a collisional mechanism indicates that molecular nitrogen may be playing a role in the degradation of polymers in space and that collisional processes could be exploited in etch environments in order to enhance etch rates and, perhaps, even improve etch characteristics.

ETCHING OF HYDROCARBON POLYMERS WITH HYPERTHERMAL NEUTRAL BEAMS

by

James William Seale

A thesis submitted in partial fulfillment
of the requirements for the degree

of

Master of Science

in

Chemical Engineering

MONTANA STATE UNIVERSITY – BOZEMAN
Bozeman, Montana

August 1998

APPROVAL

of a thesis submitted by

James William Seale

This thesis has been read by each member of the thesis committee and has been found to be satisfactory regarding content, English usage, format, citations, bibliographic style, and consistency, and is ready for submission to the College of Graduate Studies.

Dr. Bonnie Tyler (Signature) 8/19/98 Date

Approved for the Department of Chemical Engineering

Dr. John Sears (Signature) 8/19/98 Date

Approved for the College of Graduate Studies

Dr. Joseph J. Fedock (Signature) 8/20/98 Date

STATEMENT OF PERMISSION TO USE

In presenting this thesis in partial fulfillment of the requirements for a master's degree at Montana State University – Bozeman, I agree that the Library shall make it available to borrowers under the rules of the Library.

If I have indicated my intention to copyright this thesis by including a copyright notice page, copying is allowable only for scholarly purposes, consistent with "fair use" as prescribed in the U.S. Copyright Law. Requests for permission for extended quotation from or reproduction of this thesis in whole or in parts may be granted only by the copyright holder.

Signature James W. Seale

Date 19 August 1998

ACKNOWLEDGMENTS

I greatly appreciate Dr. Timothy Minton for providing guidance and support in the development of the laboratory experiments that support this thesis. I also appreciate the leadership of Dr. Bonnie Tyler.

I thank Dr. Joe Perry, at the Jet Propulsion Laboratory, in Pasadena, California, for the polyimide samples used in the neutral beam etching experiment. I would like to thank Dr. Rick Buss at Sandia National Labs, in Albuquerque, New Mexico. He provided prompt support in the design and implementation of the thermal source of oxygen atoms and donated the RF generator and variable capacitor to our research group. I also thank Agnes Tempez and Dr. A. Bensaoula at SVEC, the University of Houston, for providing the Kapton samples. Additional thanks go to Angela Frandsen for her assistance in the laboratory.

This research was funded by a grant from the Department of Defense Experimental Program for the Stimulation of Cooperative Research (DEPSCoR) administered by the Air Force Office of Scientific Research (Grant No. F49620-96-0276). Additional funding was provided by a grant from Ionwerks, a research firm in Houston, Texas.

Finally, I would like to express my appreciation for my wife, Kris, who has provided enduring love, patience, and support. Also, I thank my parents, Jerry and Carolyn Seale, for their love and wise advice throughout my life.

TABLE OF CONTENTS

TABLE OF CONTENTS – Continued

LIST OF TABLES

LIST OF FIGURES

Figure Page

LIST OF FIGURES – continued

LIST OF FIGURES – continued

Figure Page

ABSTRACT

The erosion of polymeric materials in atomic oxygen environments is important 1) as an aspect of materials degradation on spacecraft in low Earth orbit (LEO) and 2) in certain etch processes in the manufacture of microelectronic devices that involve the patterning of polymer films. In this work, directed beams of energetic neutral species have been tested as a means to achieve etching results that are superior to those obtained in plasma environments. In addition, molecular beam techniques have been employed to probe the mechanisms by which polymers erode. A laser detonation source, originally developed for ground-based testing of candidate spacecraft materials, was used to generate fast neutral species for these experiments. This source was coupled to a crossed molecular beams apparatus that has a rotatable mass spectrometer detector for analysis of volatile etch products.

The etching of a polyimide was conducted with a neutral beam of oxygen atoms created from precursor gases of N_2O and O_2. The results described in this thesis demonstrate the effect of incident energy and flux on the anisotropy and surface roughness of etched features. Etch anisotropy (undercutting) was minimized with the use of highly directional incident reactive species with high kinetic energies. Surface roughness was minimized with a higher reactive species flux on the surface and lower incident kinetic energies. The beam created from N_2O etched more rapidly and yielded superior etch characteristics as compared to the beam created with O_2.

Mechanistic studies were designed to investigate the material removal mechanism during steady-state etching. A effusive source of oxygen atoms was designed, built, and characterized. This source was used to direct a continuous stream of near-thermal oxygen atoms at a polymer surface, in order to approximate the steady-state oxidation conditions that would occur during plasma etching. The removal rate of a major reaction product, CO_2, was significantly enhanced when pulsed beams of hyperthermal nonreactive species were directed at the continuously oxidized surface. Hyperthermal beams of N_2 and Ar, with incident kinetic energies in the range 8 to 16 eV, apparently assisted in the release of CO_2 through a collisional process that became important above 10 eV. The signal intensity of the volatile CO_2 product increased exponentially with increasing incident energy. The large increase in CO_2 removal rate through a collisional mechanism indicates that molecular nitrogen may be playing a role in the degradation of polymers in space and that collisional processes could be exploited in etch environments in order to enhance etch rates and, perhaps, even improve etch characteristics.

CHAPTER ONE

INTRODUCTION

Energetic oxygen atoms react with hydrocarbon polymers to produce volatile products, and this process leads to material erosion. This erosion process is studied for several important and diverse reasons.

First, polymer spacecraft components erode due to collisions with energetic atomic oxygen in low Earth orbit (LEO). Therefore, there have been numerous studies to predict the durability of polymeric materials exposed to the LEO environment [1-3]. Ground-based testing provides important insight into how different materials behave when subjected to atomic oxygen attack. Molecular dynamic modeling also provides information which predicts erosion behavior, but modeling parameters depend on the material removal mechanisms, which remain unclear.

Secondly, when this erosion process is controlled by a patterned, protective mask, the process is considered etching. Oxygen plasmas, which contain reactive oxygen atoms, are used extensively to transfer lithographically defined features to an underlying polymer in microelectronic device fabrication [4-11], and there is growing research in patterning electro-optic polymers for low loss optical waveguides by using oxygen plasmas [12]. Reactive ion etching (RIE) using an oxygen plasma is the industrial

method of choice for etching features in polymers. However, limitations of RIE such as: microscopic nonuniformities [13], sidewall bowing and undercutting [14], and charge and ion-bombardment damage [15]; drive researchers to understand the etching mechanism more clearly. These limitations are associated with characteristics of plasmas and can be eliminated with the use of a neutral, directed beam of reactive particles. This approach was realized after polymer exposure to directed O atoms in LEO yielded eroded features and produced straight sidewalls [16]. A neutral beam of oxygen atoms would provide a means of studying not only the etched polymer features from a well-characterized beam but also the atom-surface interactions that lead to volatile products leaving the surface.

Experiments were conducted which exposed a polyimide to a beam of atomic oxygen. The atomic oxygen was produced from N_2O or O_2 precursor gases. Results indicated that a beam produced from N_2O etched more rapidly with smoother surface roughness than a beam produced from O_2. With the N_2O beam, the energy of the incident beam and the relative flux of the beam were varied, and the resulting etched features were analyzed qualitatively with a scanning electron microscope. A qualitative explanation of the results based on inelastic scattering experiments is also presented [17, 18].

In order to determine additional and precise information about the mechanisms which created the observed etched features, researchers have investigated the mechanism of volatile species production by measuring product time-of-flight distributions upon impact of the atomic and molecular oxygen beam. The experiment performed by Brinza *et al.* raised additional questions about the mechanism which produces CO_2 as the volatile species during etching of Kapton, a polyimide used both in space and in microelectronics

because of its superior thermal control characteristics [16]. Since ground-based testing of polymers exposes the surface to high energy oxygen molecules as well as to reactive oxygen atoms, the relatively nonreactive O_2 may participate in the material removal process but not directly react with the surface. We propose that when a nonreactive species impinges on the surface of a polymer that is undergoing continuous erosion from atomic oxygen, sufficient energy transfer from the incident species to the surface causes the release of volatile products via several possible mechanisms.

The apparatus used in these experiments, the data collection system, and the operation of the scanning electron microscope for surface topography analysis are described in Chapter 2. Chapter 3 provides background to important etching characteristics involved when a polyimide is etched with a neutral beam of reactive particles. In order to investigate the collisional processes that may exist, a new source of oxygen atoms was designed, characterized, and directed at polymer samples. The primary function of this source is to produce a reactive layer that approximates the surface of the polymer under steady state erosion conditions. The details of the new source are described in Chapter 4. Chapters 5 and 6 detail the experiments where polymer samples (polystyrene and Kapton) were subjected to the thermal source of oxygen atoms and were struck by an energetic, nonreactive beam. When the beam struck the oxidized polymers, reaction products (CO and CO_2) were released from the surface. Time-of-flight distributions of CO_2 were collected with a quadrupole mass spectrometer.

CHAPTER TWO

EXPERIMENTAL METHODS AND ANALYSIS

Experimental Apparatus

The experiments presented here were conducted with a crossed molecular beams scattering chamber that houses a rotatable quadrupole mass spectrometer (QPMS). The design of the apparatus is presented in detail by Lee *et al.* [20]. This apparatus provides unique diagnostic capabilities because of the rotatable detector which can measure the velocity and angular distributions of products from beam-surface experiments. A laser detonation source provides directional, hyperthermal species that originate in a differentially pumped source chamber [21]. Materials can be placed in the source chamber for relatively high flux exposure to the hyperthermal beam or on a manipulator in the main scattering chamber for controlled beam-surface experiments. A schematic diagram of the hyperthermal beam source, the main scattering chamber, and the detector, is shown in Figure 1.

Laser Detonation Source

The laser detonation source can produce a pulse of hyperthermal particles that expand outwards from the inside of a conical nozzle. This source was designed by

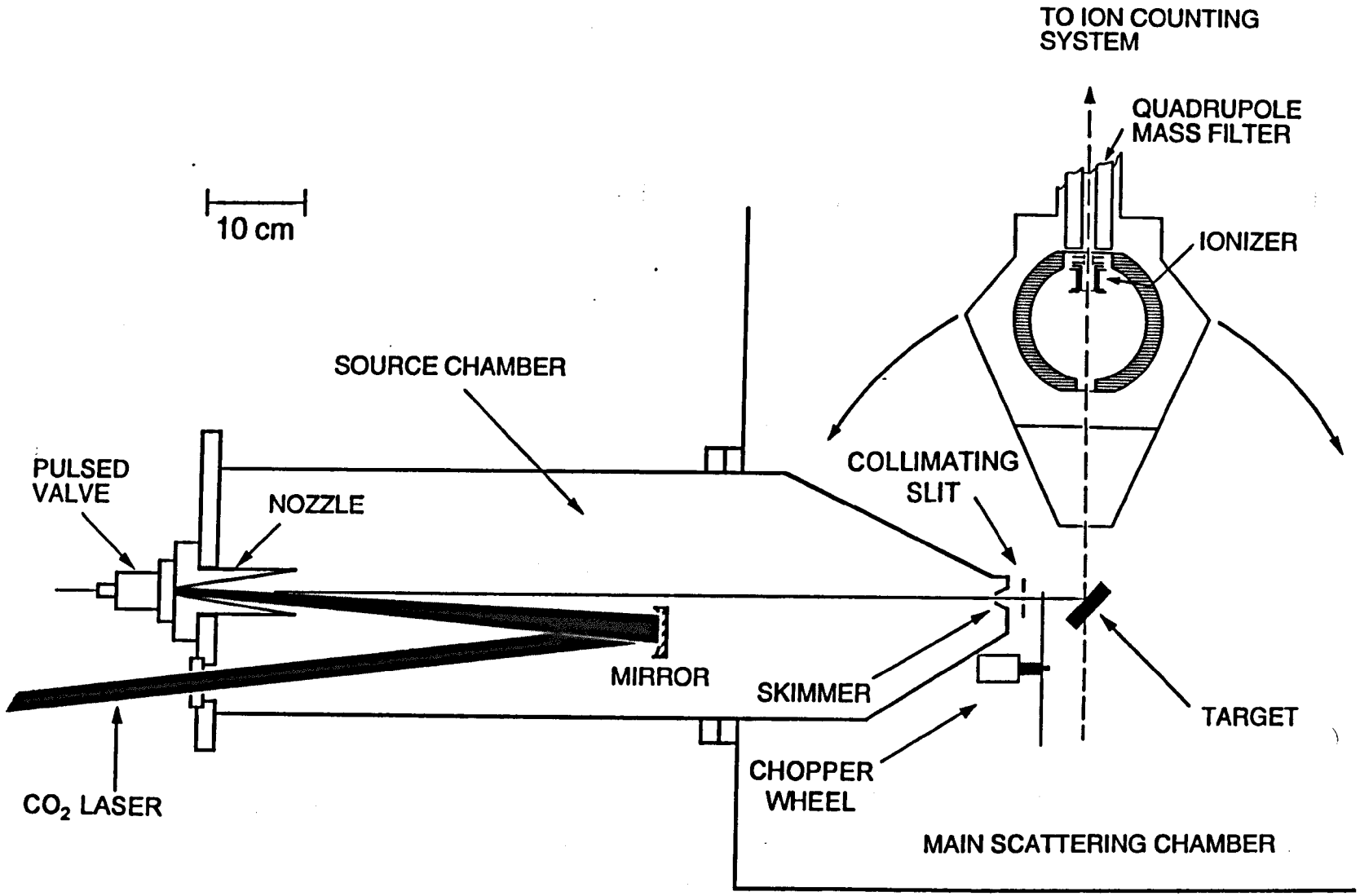

Figure 1. Schematic diagram of the hyperthermal beam source, main scattering chamber, and detector.

Krech at Physical Sciences, Inc. A piezoelectric-controlled pulsed valve [22] opens for approximately 125 μs and allows a precursor gas (for example, SF_6, O_2, N_2O, or Ar) at approximately 8-10 atms to enter the conical nozzle through a 1.0 mm hole in the apex of the cone. After approximately 200 μs from the opening of the pulsed valve, a CO_2 TEA laser (wavelength of 10.6 μm, Alltec-851) fires and is focused by a gold mirror into the center of the conical nozzle. The laser power is typically ~5.2 J/pulse, and the repetition rate of the source is 1.9 Hz. The laser induces a breakdown in the precursor gas, and heats the resulting plasma to >20,000 K. The hot plasma then rapidly expands out of the cone. The density of the expanding plasma is sufficient to induce efficient electron-ion recombination and inefficient atom-atom recombination, creating a beam of neutral particles traveling through the chamber as if emanating effectively from a point source. During operation of the source, pressure can be measured with an ionization gauge and reaches ~5 x 10^{-4} torr in the source chamber during the beam pulse. The beam pulse travels into the main scattering chamber through a 3-mm-diameter skimmer, which is 80 cm from the apex of the conical nozzle. For beam-surface experiments, the beam passes through a 1.8-mm-diameter collimating aperture and a velocity-selecting chopper wheel. The chopper wheel is a disk which has four slots precision-machined at 90° angles to each other. A slot passes between a light emitting diode and a photodiode that are 90° from the beam axis, thus creating a voltage signal signifying the instant another slot is aligned with the beam axis. The slot position can be synchronized with the repetition rate of the pulsed beam, thus selecting a narrowed distribution of the entire beam. The source

chamber is differentially pumped by a 10 inch diffusion pump (Varian, VHS-10) with a liquid nitrogen trap.

Detector

Time-of-flight (TOF) measurements are collected with the QPMS equipped with a Daly ion counter [20, 23]. Ions are produced in an electron bombardment ionizer that was designed by Brink [24], and then they were mass selected with a quadrupole mass filter. The Daly detector utilizes an aluminum coated stainless steel electrode, or "doorknob," with a high negative potential, -15kV to –30kV. Positive ions which are mass filtered slam into the "doorknob" emitting several secondary electrons per ion, which are immediately repelled away from the electrode in the same electric field. Then an electron strikes an aluminum coated plastic scintillator producing several photons; the photons emitted by the scintillator are then converted back to an electronic signal by a photocathode via the photoelectric effect [25]. The photocathode is part of the photomultiplier tube (PMT) which finally amplifies the signal above a threshold limit set by a discriminator. The discriminator threshold prevents stray photons from triggering the counter. The discriminator pulses are detected by the multichannel scaler (MCS), which sums the number of pulses in a specified time interval, or channel. The MCS also collects these data for a specified number of channels. When the MCS receives the next start trigger, it returns to time zero and sums the contents of the present channel with that of the preceding channels corresponding to the respective time interval.

Because velocity distributions and energy calculations depend on the actual time it takes a particle to travel from its origin to the ionizer, the time scale of all species

collected by the detector must be offset. For example, the ion flight time must be subtracted from the signal since all ions of the same mass travel at the same velocity from the ionizer through the quadrupole mass filter to the ion counter. Upon ionization, the species are accelerated by an electric field to the mass filter. Here, the potential energy to kinetic energy conversion:

$$E = zeV = \frac{1}{2}mv^2 \tag{1}$$

yields the relationship,

$$t = \frac{l}{\sqrt{2eV}}\sqrt{\frac{m}{z}} = \alpha\sqrt{\frac{m}{z}}. \tag{2}$$

Therefore, the time it takes an ion to travel from the ionizer to the ion counter is only a function of the square root of the mass-to-charge ratio, *m/z*. Therefore, the constant, α, is only a function of the detector conditions.

Experimental Techniques

Exposure experiments are conducted by placing a sample inside the source chamber, normal to the axis of the beam, and 30 to 50 cm away from the apex of the nozzle. A change in the distance from the sample to the nozzle represents a change in the relative flux of particles on the surface by the relationship: flux $\propto d^{-2}$, where d is the distance. The flux on a surface 30 cm from the apex is approximately 10^{15} particles cm^{-2} sec^{-1}, depending mostly on the precursor gas. The QPMS may be rotated so that the detection axis is aligned with the center of the beam pulse. This configuration permits the characterization of the hyperthermal beam. A 0.12-mm-diameter detector

aperture must be used since the beam is intense and could cause gas buildup in the differentially pumped ionization region.

The hyperthermal beam may also be used to investigate beam-surface dynamics. Samples are mounted on a manipulator such that the sample surface normal is contained in the plane of the detection and incident beam axes. Also, the manipulator is positioned such that the rotation axis of the sample is coincident with the detector rotation axis. The sample is located 92 cm from the apex of the conical nozzle. The QPMS, with three differential pumping zones, can be rotated about the sample and detect the velocity and angular distributions of inelastically scattered and reactively scattered products from beam-surface interactions. The distance from the surface to the detector ionizer is 33.9 cm, and the detector views a 3-mm-diameter spot on the surface. The detector was designed to obtain TOF distributions which correlate to the true kinetic energy of the detected species.

Analysis Techniques

Scanning Electron Microscopy

The topography of polymer samples etched by the hyperthermal beam source were analyzed with a scanning electron microscope (SEM). The polymer samples were spin-coated on silicon substrates. A cross-section of the etched features could be obtained by cleaving the substrate in a precise location. The etched sample was then coated with a gold-palladium alloy to prevent charging effects characteristic of insulating

materials. The SEM apparatus used for the analysis was located at the Image and Chemical Analysis Laboratory (ICAL) at Montana State University.

Scanning electron microscopy offers magnification up to 100,000x with a spatial resolution of 10 nm. The depth of field depends on the particular apparatus and the working distance (the distance from the sample to electron detector) but is typically one μm. The SEM apparatus consists of an electron gun and focusing devices operating in a vacuum. The electrons can be accelerated up to 40 keV but are typically accelerated to 15 keV or less. Higher electron energy is required for acceptable resolution at higher magnification. Electron lenses produce a beam of electrons with a small diameter, and the beam is rapidly scanned across the area of interest. The electrons interact with the near-surface region of the sample and produce secondary electrons. As the beam moves across the surface, the intensity of variation in the emitted secondary electrons due to the surface topography can be viewed on the screen as an image [26].

TOF Distribution Analysis

TOF distributions that are collected by the MCS, originate as number density functions versus time, $N(t)$ versus t. As mentioned previously, the time scale of raw data must be corrected so that time zero represents the actual time at which the detected species leaves a distinct position. For example, species begin at the apex of the conical nozzle for beam TOF distributions, and products from beam-surface interactions begin at the sample surface upon impact of the impinging beam. Since the distance that species travel and the time interval that it takes for the species to travel that distance are known, the TOF data represent distributions of product velocities.

In the determination of species energy from the TOF data, the *N(t)* versus *t* signal must be converted to a flux distribution function versus the energy, *P(E)* versus *E*. The flux distribution function is proportional to the number density function by the relation:

$$P(E) \propto t^2 N(t). \tag{3}$$

The energy of the species (*E*) may be directly determined from the species velocity.

It is also common to compare the relative intensities of two or more beams or products. To integrate the intensity of a TOF distribution, the number density distribution must be converted to a flux-weighted distribution. The flux-weighted distribution is proportional to the number density function by the following relation:

$$I(t) \propto \frac{N(t)}{t}. \tag{4}$$

Therefore, the integrated intensity of a distribution is

$$\int I(t)dt = \int \frac{N(t)}{t} dt \approx \Sigma \frac{N(t)}{t}. \tag{5}$$

CHAPTER THREE

NEUTRAL BEAM ETCHING OF A POLYIMIDE

Introduction

As the number of applications of polymer etching continues to grow, characteristics of the etching process will have to be better understood. State-of-the-art processes for the etching of polymers utilize plasmas, but as the density of features on microelectronic devices increases, plasma etching will need several process improvements to maintain the "state-of-the-art" status. Aspect ratio dependent etching (ARDE) refers to a dependency of the etch rate on the depth and line width of the feature. Several of the causes of ARDE arise from process characteristics only attributed to plasmas; therefore, a neutral beam etching technique could offer unprecedented results in the etching of polymers [13]. Some drawbacks of plasma etching of polymers may be improved with a neutral beam technique. The neutral beam technique could also provide information on (1) the evolution of the sidewall profile, (2) the evolution of surface and sidewall roughness, and (3) the capability of tapered etching for specific applications (for example, the coupling of a smaller polymer waveguide to a larger glass fiber). In this experiment, neutral beams containing oxygen atoms, produced with the laser detonation

source, etched a polyimide material under various conditions. This information provides preliminary information on the capability of neutral beam etching of polymers.

Background

The idealistic case of the etching process is shown in Figure 2. A directed beam of energetic neutrals impinges on the surface with normal incidence and etches the material not protected by the aluminum mask. The material in this etching analysis is a 4-6 μm-thick layer of polyimide that was spin-coated onto a silicon substrate. After etching, a feature is formed and sidewalls are straight. It would also be ideal if the etched surfaces were completely smooth.

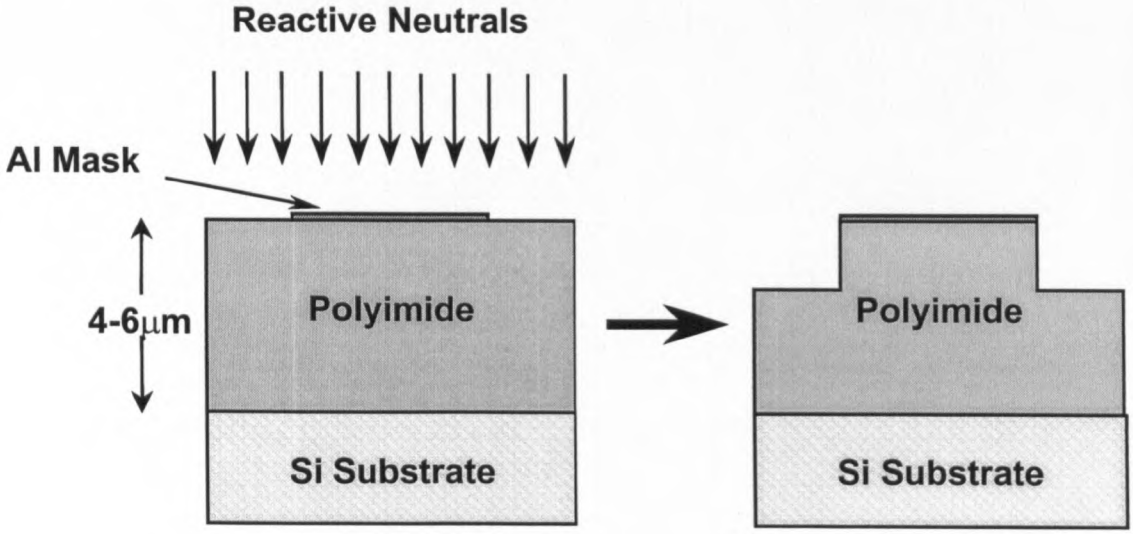

Figure 2. Idealistic portrayal of the etching process.

A diagram illustrating realistic characteristics is shown in Figure 3. After etching, there is undercutting of the sidewall, and the etched surfaces are rough. The undercutting of the polymer refers to the material that was removed from beneath the mask.

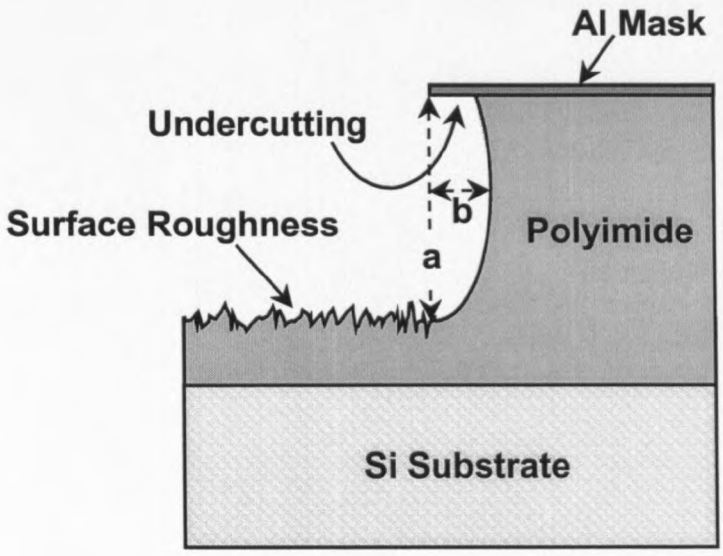

Figure 3. Realistic depiction of etching characteristics.

Undercutting can be quantified by *anisotropy* which is the ratio of the etch depth to the greatest distance from the edge of the mask to the polymer sidewall. This ratio is shown in Figure 3 as *a/b*. The roughness of the surfaces is determined qualitatively with scanning electron microscope images; however, it may also be determined quantitatively with atomic force microscopy.

Exposure Conditions and Preliminary Results

Neutral, energetic particles were created with the laser detonation source described in Chapter 2. Initially, O_2 was used as the precursor gas and a beam of atomic oxygen and molecular oxygen was produced. Several exposures were performed and analyzed with SEM. The preliminary results indicated substantial surface roughness of cone-like features. We then attempted to produce reactive O atoms with a different

precursor gas, N_2O. We were able to obtain very high energies and sufficient dissociation with the N_2O gas. And after etching, the cone-like features were considerably minimized. Figure 4 shows the energy distribution of the O and O_2 for one exposure condition. A polyimide sample was etched for 17 hours (~110k beam pulses) at a distance of 50 cm from the apex of the conical nozzle with the beams in Figure 4. The

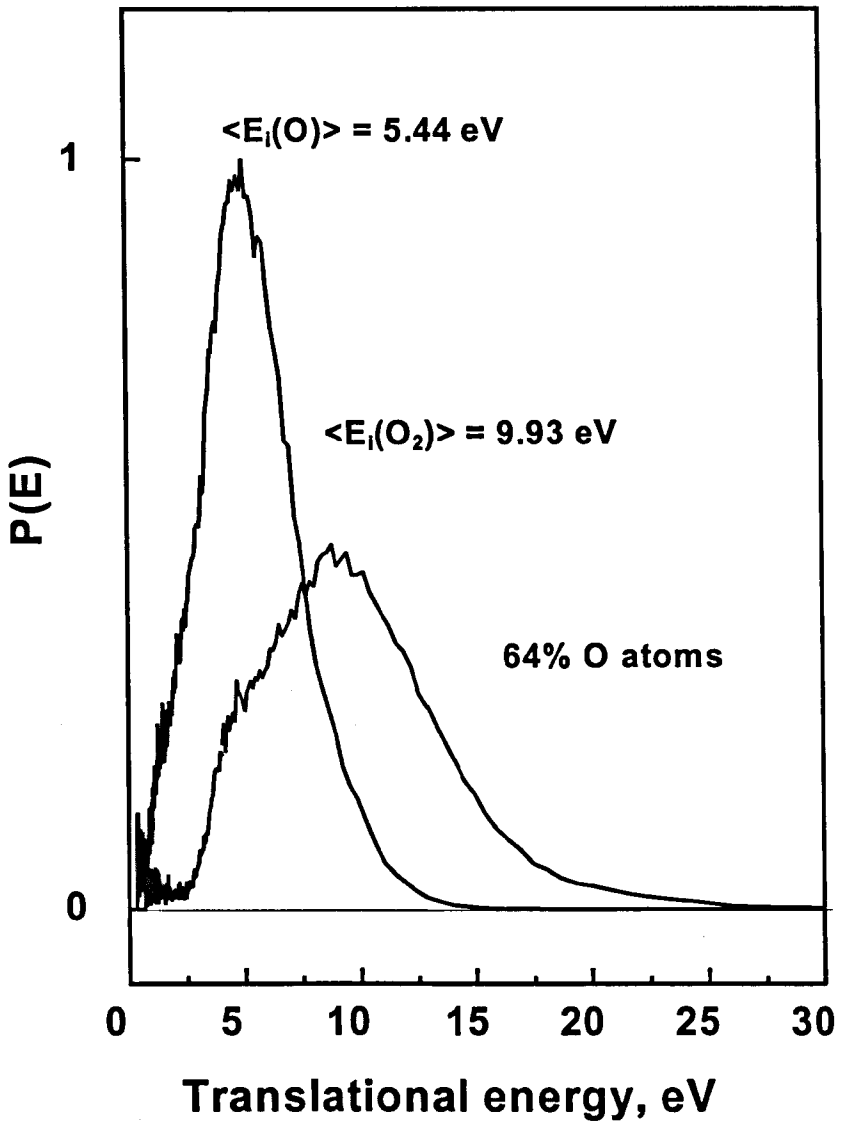

Figure 4. Energy distributions of O and O_2 during polyimide exposure.

intensity of the O_2 beam was scaled to the ratio of the integrated intensity of molecular oxygen to the integrated intensity of the atomic oxygen. The beam was 64% O atoms. Figure 5 shows the energy distributions for the N_2 and O components created from the N_2O gas. There may have been N atoms in the beam, but signal at a m/z = 14 would partly be N_2 cracking and unresolved O atoms. In Figure 5, the beam intensities were

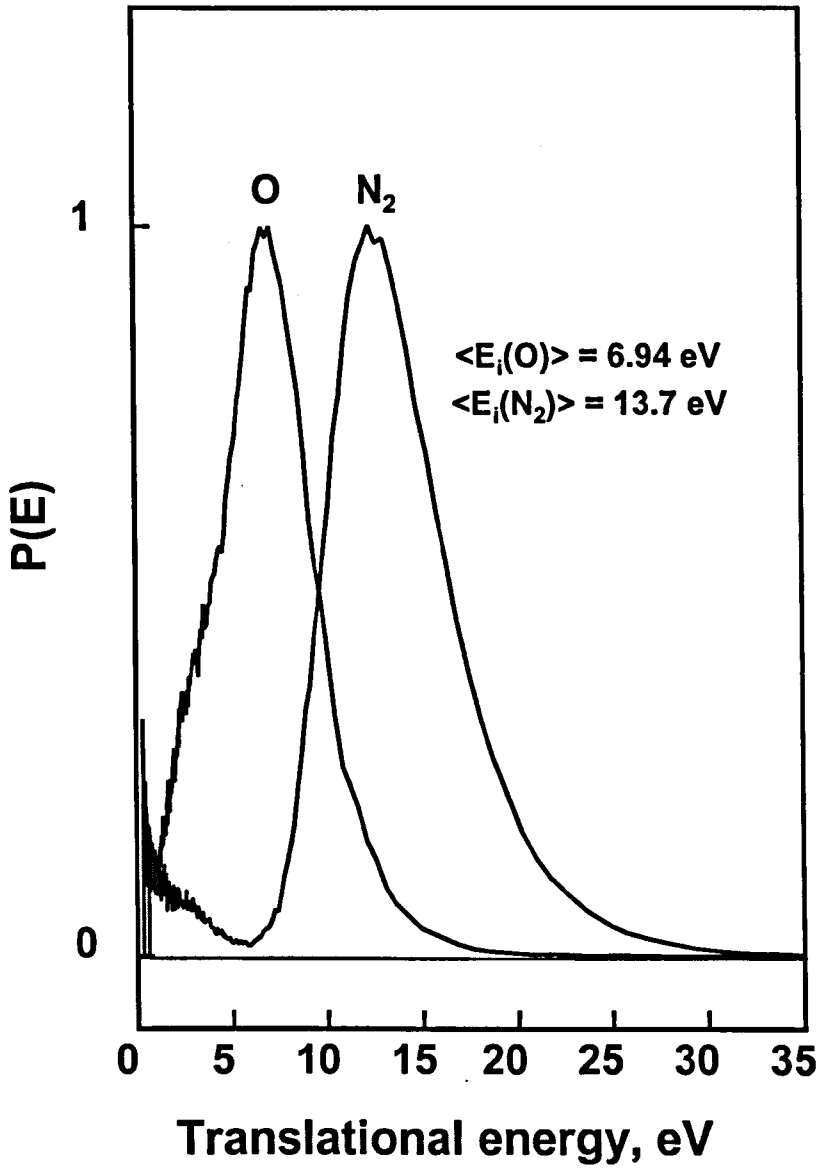

Figure 5. Energy distributions for N_2 and O during polyimide exposure.

both normalized to one. Both groups of beams have an atomic oxygen component and a relatively nonreactive species (N_2 or O_2). Similarly, another polyimide sample was etched with the neutral beams shown in Figure 5.

Figure 6 shows the SEM photographs of these cleaved samples, which illustrate the comparison of the surface roughness with respect to beams produced from O_2 and from N_2O. In Figure 6, the surface roughness of the O_2-beam-etched sample is on the order of one micrometer (μm), while the N_2O-beam-etched sample shows much smaller surface roughness. From these results, the N_2O beam was chosen for further neutral beam etching studies.

Results and Discussion

Dependence of Undercutting on Incident Energy

Two samples were etched by the neutral beam with the same source-to-surface distance, 27.5 cm, and with different energies. Only the energy of the O atoms is reported, but all species of the beam travel at similar velocities; therefore, if the average energy of O atoms is higher in one beam, the average energy of the N_2 component would be proportional. The SEM photo in Figure 7 shows a sample etched with an average O energy of 4.6 eV. The *anisotropy* ratio was determined to be 2.7, indicating a bowed sidewall. The photo in Figure 8 shows a sample etched with a 9 eV O-atom beam, and the feature has an *anisotropy* ratio of 3.6, which indicates the sidewall is less bowed and less undercut than the sample etched with the less energetic beam. Therefore, as the energy increased, the sidewall of the feature became straighter.

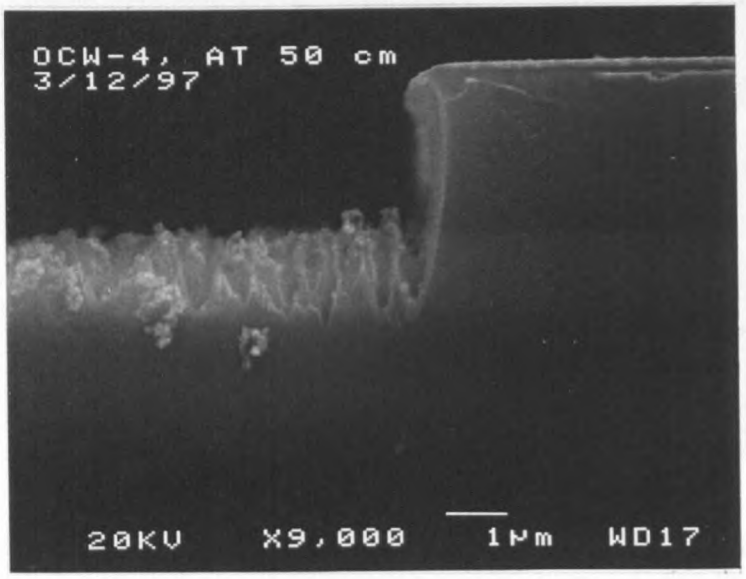

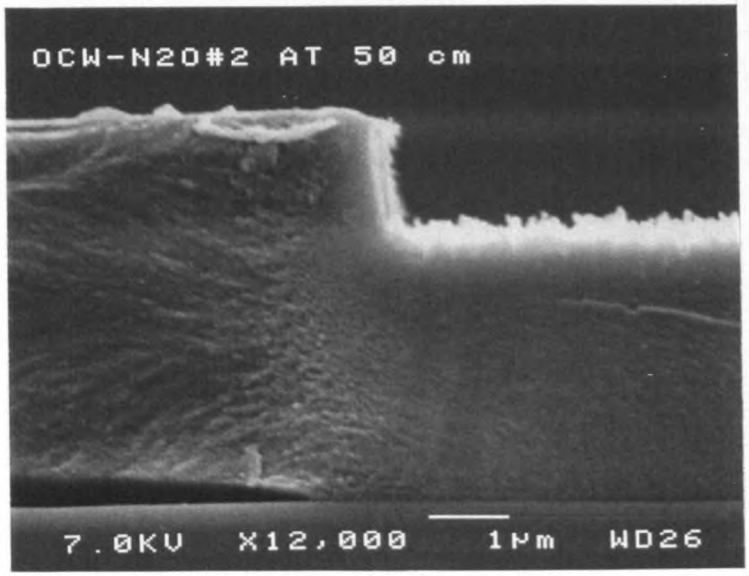

Figure 6. Comparison of etched features from O_2 and N_2O beams. The top photo shows an etched polyimide sample exposed to the O-atom beam shown in Fig. 4. The bottom photo shows the etched polyimide feature exposed to the O-atom beam in Fig. 5. Notice the difference in surface roughness between the two samples.

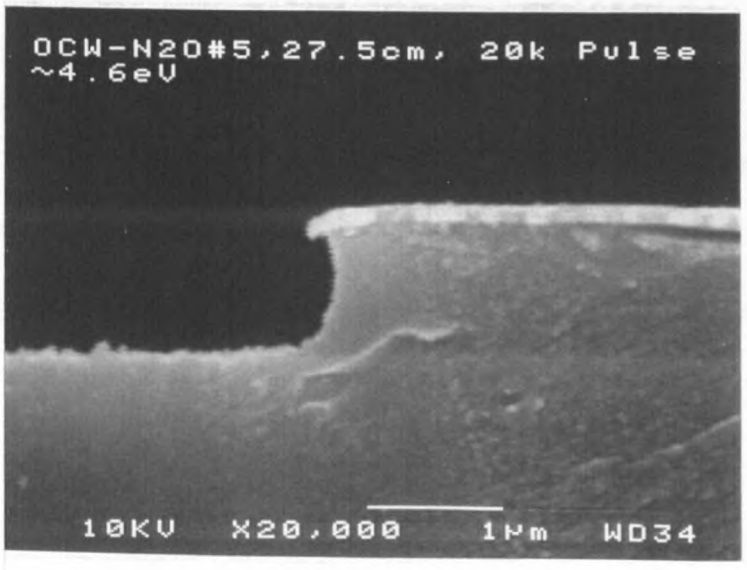

Figure 7. SEM photo of a feature that was etched 27.5 cm from the apex of the source nozzle at an average O-atom energy of 4.6 eV. The *anisotropy* ratio is 2.7.

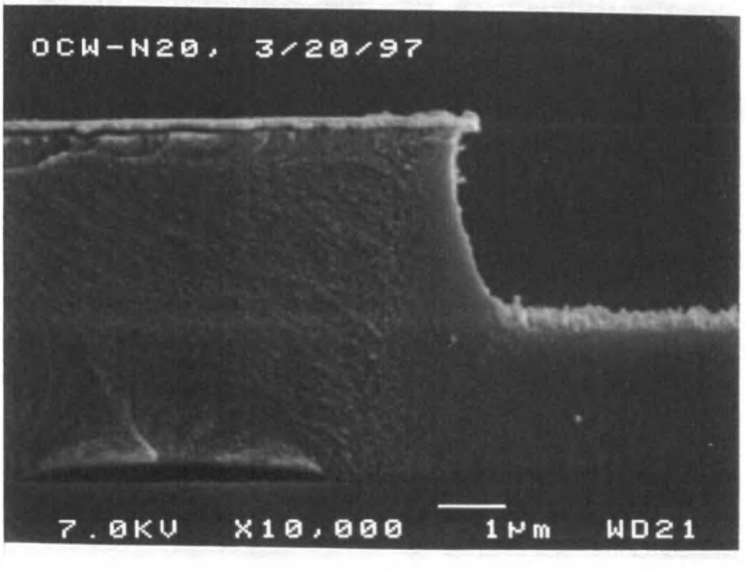

Figure 8. SEM photo of a feature that was etched 27.5 cm from the apex of the source nozzle at an average O-atom energy of 9.0 eV. The *anisotropy* ratio is 3.6.

Dependence of Undercutting on
Source-Sample Distance

A set of samples was etched with beams having the same average O atom energy, 9 eV, but the distance from the source to the sample was changed from 27.5 cm to 50 cm. Therefore, the etched features show the dependence of undercutting on the variation in the relative flux of neutral particles on the surface. The photo in Figure 8 again shows an *anisotropy* ratio of 3.6 for a feature that was etched with a 9 eV O-atom beam and that was placed 27.5 cm from the source. The SEM photo in Figure 9 shows the *anisotropy* ratio to be increased to 7.0 when the sample was moved to a distance of 50 cm away from the source. Therefore, the sidewall profile became much straighter as the source-sample distance increased.

Qualitative Explanation of Undercutting

Two factors contribute the undercutting effect on the sidewall formation during neutral beam etching of the polyimide: (1) inelastic gas-surface scattering and (2) gas-phase scattering. The role of inelastic gas-surface collisions on the formation of sidewall profiles has been reported by Hwang *et al.* for the etching of silicon with fluorine atoms [17]. The qualitative explanations below describe the undercutting characteristics and are consistent with these reported effects of inelastic collisions. In Figure 10, a reactive species impinges the surface and inelastically scatters with an appropriate exit angle to react with the sidewall surface, thus creating an undercut feature. Inelastic scattering at these large exit angles is reduced when the incident beam has higher translational energy, as a result of a higher reaction probability on the first impact.

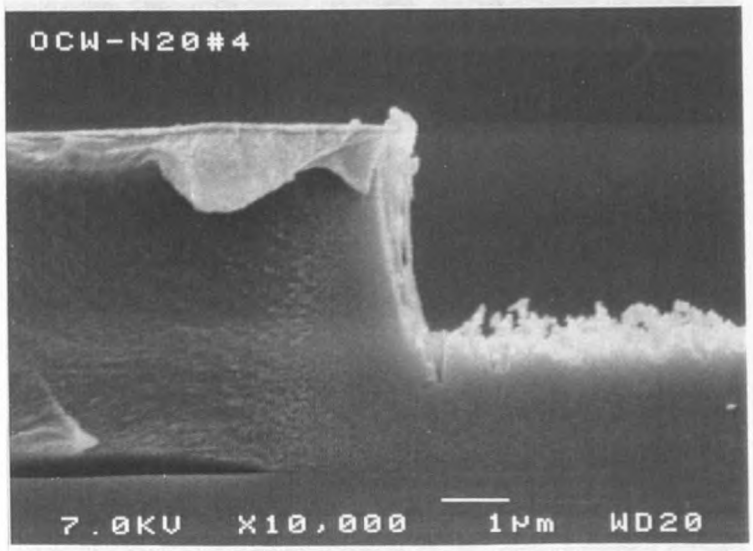

Figure 9. SEM photo of the sidewall of a feature etched by a beam with 9 eV O atoms at a distance of 50 cm from the source. The *anisotropy* ratio here is 7.0.

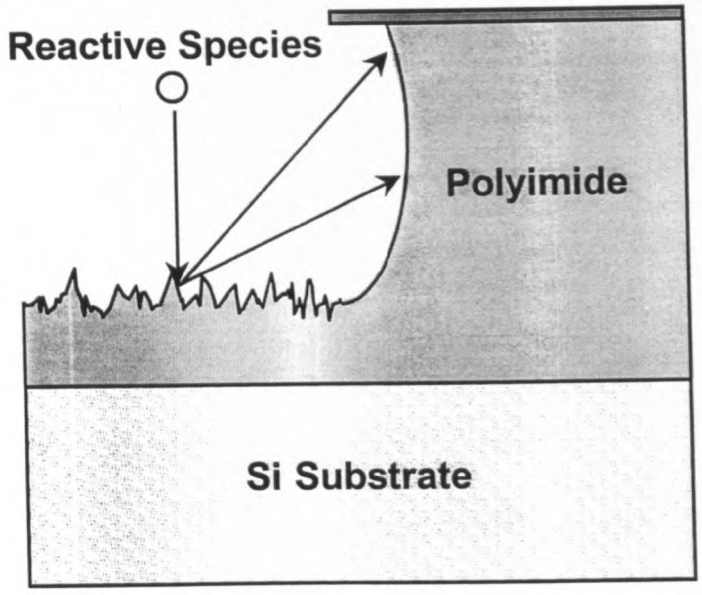

Figure 10. Inelastic gas-surface scattering leading to sidewall reactions.

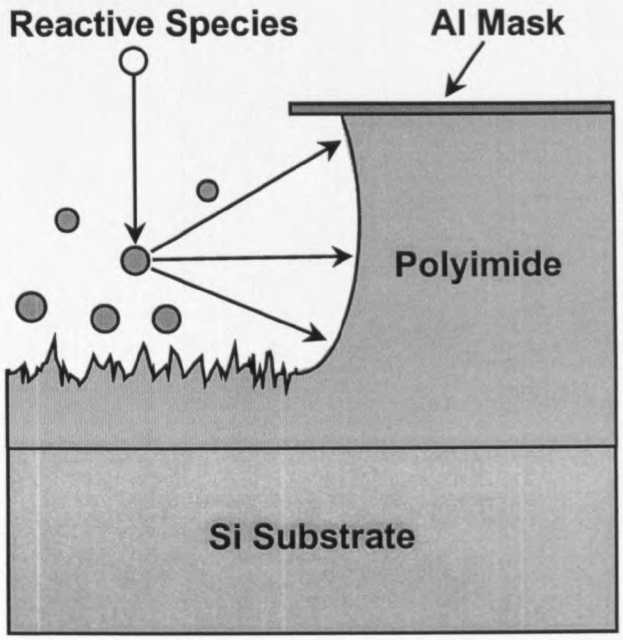

Figure 11. Gas-phase scattering impact on undercutting.

In Figure 11, a reactive species collides with an unreacted species that has scattered off the surface or with a reaction product released from the surface. The deflected reactant may impinge on the sidewall with sufficient energy to react. The probability of this undercutting effect decreases as the source-sample distance increases because of the decrease in the flux of particles on the surface.

Dependence of Surface Roughness
On Incident Energy

Figure 12 shows an SEM photo of an etched surface from a beam with an average O atom energy of 3 eV and with a source-sample distance of 27.5 cm. The photo is taken about 40 degrees from the surface normal. Figure 13 shows the surface roughness of the etched polyimide after exposure to a 9 eV O-atom beam that was also placed 27.5 cm

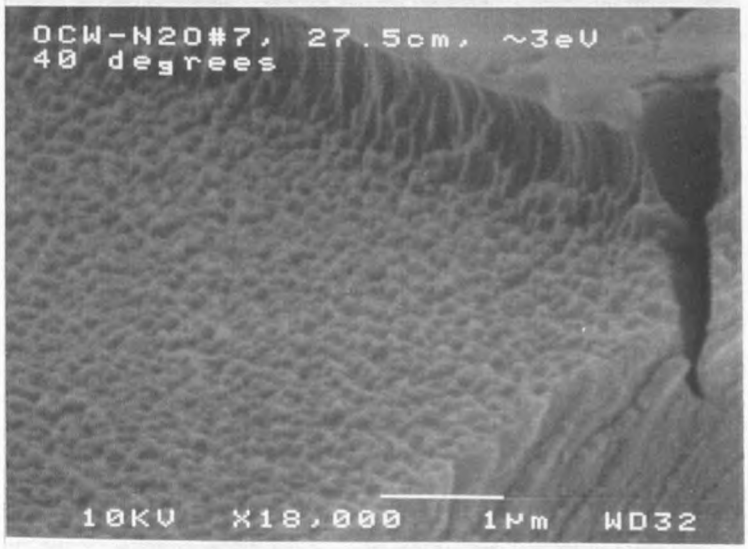

Figure 12. SEM photo that illustrates the surface roughness after etching with a 3 eV O-atom beam, 27.5 cm from the source.

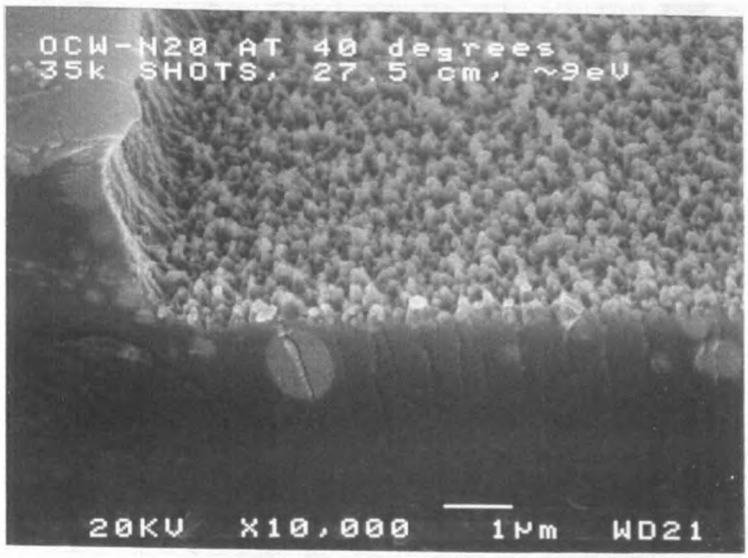

Figure 13. SEM photo that illustrates the surface roughness after etching with a 9 eV O-atom beam, 27.5 cm from the source. Note the difference in scale from Fig. 12.

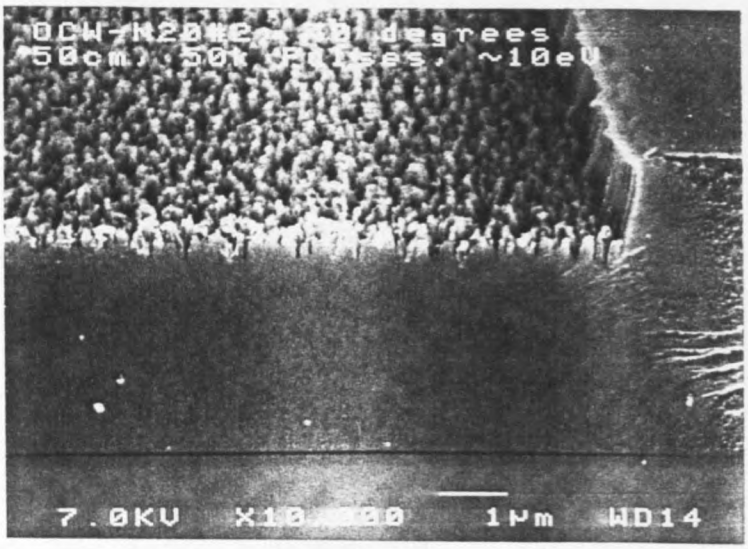

Figure 14. SEM photo that illustrates the surface roughness after etching with a 9 eV O-atom beam, 50 cm from the source.

from the source. Although the scale is different in the two photos, it is apparent that the roughness of the surface increases with a higher incident beam energy.

Dependence of Surface Roughness on
Source-Sample Distance

The SEM photos in Figures 13 and 14 show the behavior of the surface roughness as the source-sample distance is varied. Figure 14 shows the surface roughness of the etched polyimide that was exposed to a beam with an average O atom energy of 10 eV, and the sample was located 50 cm from the apex of the conical nozzle. Here, it is apparent that the roughness of the surface etched with a large source-sample distance is more defined and slightly deeper that the surface etched with a smaller source-sample distance.

Qualitative Explanation of Surface Roughness

The contributing factors leading to the evolution of surface roughness appear to be the same factors as those causing undercut sidewalls: inelastic gas-surface scattering and gas-phase scattering. Figure 15 offers an explanation for the evolution of surface roughness. As reactive neutrals from the beam begin to impinge on the surface, they create initial pit defects in the polyimide surface. As the etching process continues, the pits are propagated deeper into the polymer until a steady state process is reached. Previous gas-surface studies involving the etching of silicon with fluorine atoms provided insight into the relationship between inelastic collisions and the microscopic formation of neutral beam etched features [17-19]. Higher translational energies of impinging beam

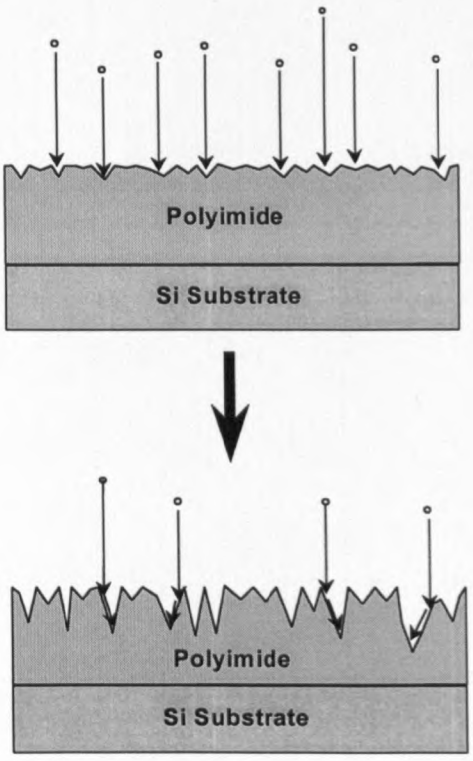

Figure 15. Evolution of surface roughness during neutral beam etching.

species result in small exit angles of inelastically scattered products. Therefore, grazing collisions with the local sidewalls in the pits concentrate reactive particles, thus increasing the secondary reactions at the bottom of the pit.

In Figure 16, the proposed effect of gas-phase scattering on the roughness of the etched surface is illustrated. Here, a reactive species collides with unreacted species and reaction products are released from the surface. These collisions reduce the directionality of impact of impinging species. The probability of these gas-phase collisions increases at shorter source-sample distances as a result of the relatively high flux of particles.

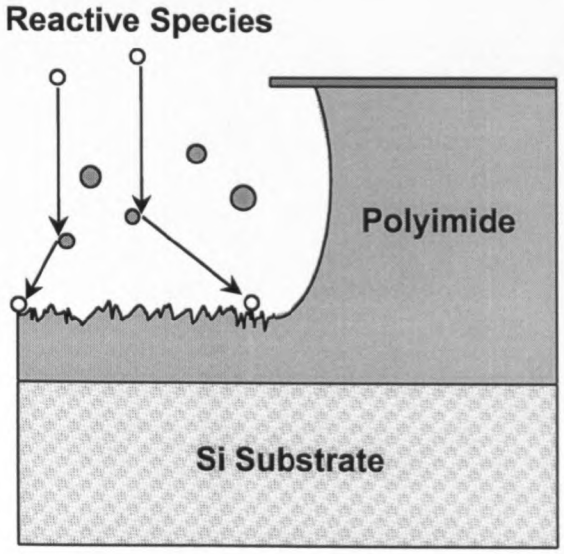

Figure 16. Surface roughness dependence on gas-phase scattering.

Sidewall Roughness

The characteristics of the etched sidewall surface are particularly important for optical applications of patterned polymers [12]. The SEM photo in Figure 17 shows the surface roughness as well as the sidewall roughness for a sample etched with a sample-

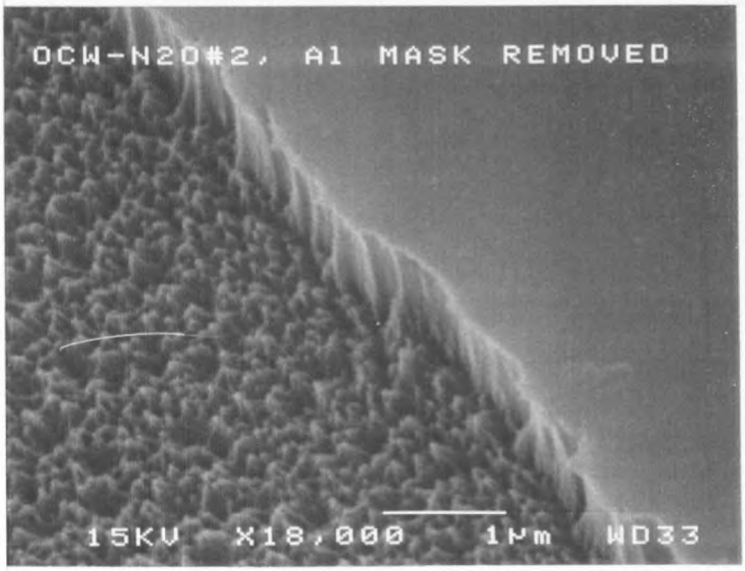

Figure 17. SEM photo that illustrates the structure of the sidewall. This sample was etched with a 9 eV O-atom beam, 50 cm from the source. Note that the sidewall striations extend down the sidewall and connect with the surface roughness features.

source distance of 50 cm and with an average O atom energy of 9 eV. The aluminum mask was removed from this sample after etching in order to view the sidewall more clearly. The aluminum mask edge had some variation, which was transferred to the ridge of the sidewall, and would be characteristic of any etch process. The key feature shown by this photo is how the fine striations on the sidewall surface extend and connect to the features associated with the surface roughness formation. By qualitative observation, the striations on the sidewall have a similar order of roughness as the cone-like structures on the surface, which is approximately 0.1μm. It is conceivable that the striations are the edges, or sides, of the surface roughness pits and are propagated during the etching process down the sidewall.

Summary

First, a hyperthermal beam, created by detonating N_2O with the CO_2 laser, etched the polyimide more rapidly and with less surface roughness than the beam produced from O_2. Qualitative results were presented which demonstrated the characteristics of neutral beam etching of a polyimide. Then, conclusions were made based on the results. The qualitative explanations given in this chapter are consistent with results that have been published for atomic fluorine incident on silicon [18, 19], including the role of inelastic scattering collisions on profile evolution [17]. Inelastic gas-surface scattering and gas-phase scattering lead to secondary reactions on the sidewall and promote undercutting. Undercutting is minimized under the following conditions: (1) minimum gas-phase scattering at long source-sample distances and (2) high translational energy of the neutral beam, which decreases the exit angle of scattered species and increases the probability that the impinging species will react on the first impact. The surface roughness is affected by the same mechanisms. The inelastic collisions of the impinging species propagate the pit-defects and cause the surface roughness. The presence of gas-phase scattering decreases surface roughness by reducing the directionality of the impinging beam species through multiple collisions. Therefore, low energy and short source-sample distances minimize the surface roughness. The sidewall roughness probably originated like the surface roughness, and the striation structure is maintained by inelastic collisions on the sidewall. The sidewall striations present a hurdle for the use of neutral beam etching of polymers for waveguide applications where smooth surfaces are required.

CHAPTER FOUR

THERMAL OXYGEN ATOM SOURCE FROM AN INDUCTIVELY COUPLED PLASMA

Introduction

During the steady state process of etching a material, the mechanisms which cause volatile products to form and leave the surface are unclear and difficult to investigate. In particular, the role of species that do not react with the surface but collide with substantial kinetic energy is uncertain. For example, the molecular beam etching method described in Chapter 3 subjected a polyimide surface to reactive oxygen atoms, nitrogen atoms, and nitrogen molecules from laser-induced dissociation of N_2O. We have the capability to determine the etching products which leave the surface and the velocity distribution of each product. However, it has been impossible to determine the effects of the nonreactive beam species, such as the N_2 component, on the erosion characteristics of polymers that are undergoing energetic atomic oxygen bombardment. Therefore, a continuous beam of thermal oxygen atoms was designed to be directed at the polymer surface. This beam can be used to create an oxidized surface layer similar to that which would be created during O-atom etching. By directing a hyperthermal beam

nonreactive species at this continuously oxidized surface, we can identify the role of collisions from energetic neutral species in the etching of a polymer.

Design of Source for Thermal Oxygen Atoms

Design criteria

To conduct experiments utilizing a new high-flux source of thermal oxygen atoms, the source must be capable of operating continuously for experiments that could extend several days. A heated nozzle would be quite reliable, but it would not produce sufficient O atoms. Therefore, the second criterion is that there be sufficient flux of O atoms on the polymer surface – greater that one monolayer (ML) per second. To satisfy this criterion, the source must be relatively close to the sample and must have a sufficient means of dissociating O_2. A source was designed which dissociates O_2 through an inductively coupled RF plasma and allows the plasma effluent to effuse from a small orifice that is placed approximately one inch from the polymer surface. The orifice of the plasma tube was chosen to be 0.5 mm; this accounted for the pumping speed of the scattering chamber, molecular flow regime, and a plasma operating pressure of approximately 100 millitorr (mT). A tube diameter of one inch was chosen after consulting Rick Buss (Sandia National Labs) who provided expert technical assistance for the design and implementation of this source. Plasmas from tubes with diameters less than one inch may be more difficult to ignite and sustain. The size of the plasma tube was also considered for reasons dealing with the power density of the plasma – power

(watts) applied to the induction coil divided by the tube volume beneath the coils. The amount of O_2 dissociation in the plasma depends mostly on the power density. However, very high power densities (well above 1 W cm^{-3}) could melt the quartz tube, especially in high vacuum. With a one inch diameter plasma tube and coils that were approximately 4 inches long, the power density ranged from 0.6 to 1.0 W cm^{-3} for operating powers of 30 and 50 W, respectively.

A schematic diagram of the plasma apparatus is shown in Figure 18. The system consisted of a radio-frequency (RF) power generator rated to 300 watts (ENI-ACG3), a 5 – 100 pF variable capacitor (Jennings), and 16 gauge bare copper wire. The copper wire was wound around a 0.875 inch OD pipe with the calculated number of coils to ensure a tight fit around the one inch quartz tube. A ground tap was also connected between the coils and the machine wall with a braided copper wire. The scattering chamber served as a pump on the tube orifice, and O_2 flow was maintained by both a vacuum regulator (Matheson) and a needle valve (Scientific Instruments).

Resonant *LC* Circuit

The *LC* circuit shown in Figure 18 operates as a resonant or "tank" circuit where the impedance of the coil, χ_L, must "match" the impedance of the capacitor, χ_C. Therefore, the circuit must be tuned until:

$$\chi_L = -\chi_C \tag{6}$$

where,

$$\chi_L = i \cdot L \cdot 2\pi \cdot F \tag{7}$$

and

$$\chi_C = \frac{-i}{2\pi \cdot C \cdot F}. \tag{8}$$

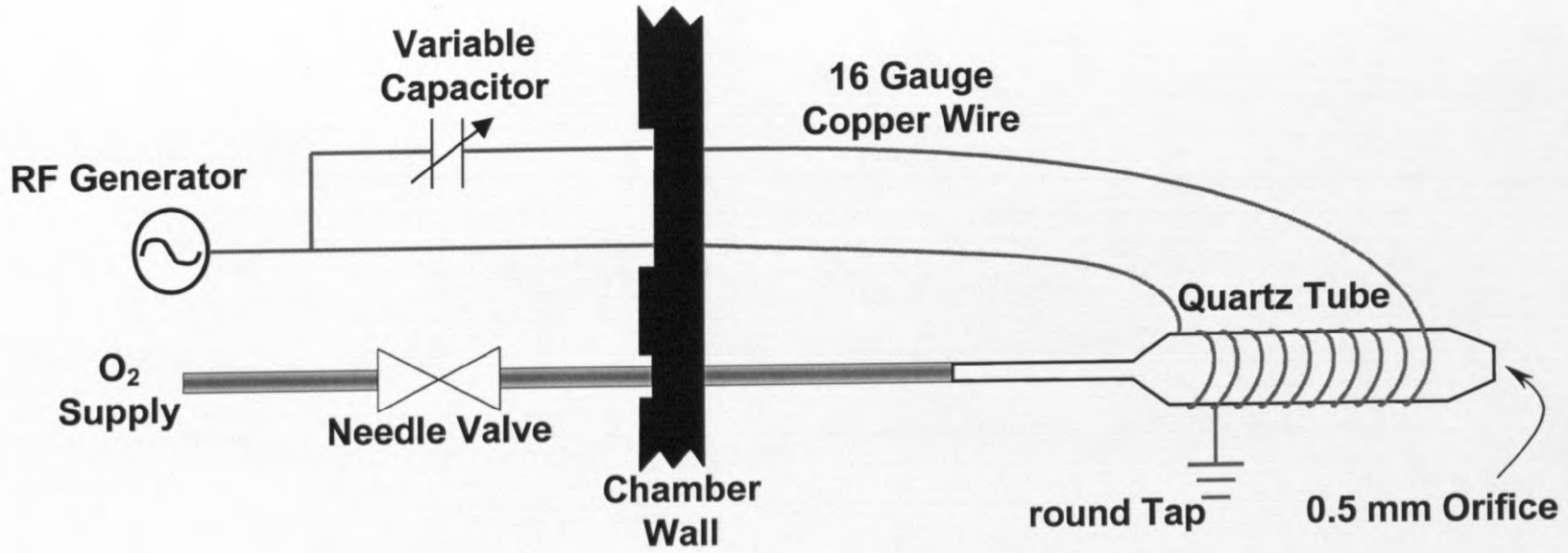

Figure 18. Schematic diagram of the inductively coupled RF plasma source.

Here, L is the inductance of a coil with given geometry and number of coil windings; F is the frequency of the RF power generator, 13.56 megahertz (MHz); and C is the capacitance at which the variable capacitor is tuned in order to produce a resonant circuit. For example, if the coil has 15 turns (N) and is 3.5 inches long (l) by one inch in diameter (d), the inductance would be:

$$L = \frac{\mu_0 N^2 \pi d^2}{4l} = \frac{4\pi \times 10^{-7} \frac{\text{Wb}}{\text{A}\cdot\text{m}} \cdot 15^2 \cdot \pi \cdot 0.0254^2 \text{m}^2}{4 \cdot 3.5 \cdot 0.0254 \text{m}} = 1.6\mu\text{H} \qquad (9)$$

where μ_0 is the *permeability of free space*. Then, the impedance of the coil would be:

$$\chi_L = i \cdot 1.6\mu\text{H} \cdot 2\pi \cdot 13.56 \times 10^6 \text{s}^{-1} = 137i\Omega . \qquad (10)$$

Therefore, capacitor must be tuned to 85.6 pF so that

$$\chi_C = \frac{-i}{2\pi \cdot 85.6\text{pF} \cdot 13.56 \times 10^6 \text{s}^{-1}} = -137i\Omega = -\chi_L , \qquad (11)$$

thus a resonant circuit is formed.

By placing a ground tap on the coil, an auto transformer circuit is produced which matches the impedance and couples the electrical power into the confined O_2 gas inside the plasma tube. The ratio of the plasma impedance (as high as 2500Ω depending on gas pressure and composition) to the power supply impedance (typically 50Ω) is proportional to the square of the ratio of the number of coil turns after the ground tap to the number of coil turns before the ground tap. Finding the ground tap position requires a trial-and-error procedure, and was determined by setting the plasma system up on a laboratory bench and pumping through the 0.5-mm-diameter orifice with a mechanical pump. It was then possible to try multiple configurations and rapidly hone in on the optimal power

coupling into the plasma, with no reflected power detected by the RF generator. The plasma apparatus was then placed into the scattering chamber where it was mounted onto a ceramic holder. The ceramic holder could be positioned onto the manipulator where the tube orifice was aligned with the detector axis, or it could be mounted to bottom of the scattering chamber and directed at a sample on the manipulator. Teflon® tubing (¼ inch OD) was used to connect the supply line of O_2 to the ¼ inch OD quartz plasma tube extension. Pressure of the supply line was monitored by a thermocouple gauge.

Characterization of Source

The plasma tube was mounted on the manipulator, and the tube orifice was aligned with the detector axis. A time-of-flight (TOF) chopper wheel with four equally spaced slots was positioned between the plasma tube and the detector aperture to modulate the continuous plasma effluent. For the characterization of the O-atom source, the wheel rotated at 160 Hz. The distance from the chopper wheel to the electron bombardment ionizer was determined to be 30.1 cm. The start signal to the multi-channel scalar was produced by the detection of light from an LED (light emitting diode) by a photodiode detector when a slot of the wheel rotated between them.

During the characterization of the source, it was important to determine the stability of the plasma. By operating the plasma at various pressures and power settings stable conditions were immediately determined. If the supply pressure dropped below 70 mT, the plasma would become faint and could not be sustained. Conversely, if the pressure was operated above 125 mT, the fraction of O atoms produced in the plasma

sharply decreased. As mentioned earlier, the power density plays the largest role in determining the extent of dissociation of O_2. Fifty watts was the maximum power that was used in order to prevent extensive heat damage to the source. It was also determined that at least 30 watts was required to sustain a stable plasma. Therefore, the time-of-flight distributions of m/z = 16 and 32 (O^+ and O_2^+, respectively) were collected at both 30 and 50 watts as well as both 75 mT and 100 mT. The TOF distributions collected at m/z = 16 are shown in Figure 19 for the four combinations of parameters, and m/z = 32 distributions are shown in Figure 20. The distributions of the beam species were plotted with the closest fit of a Maxwell-Boltzmann (MB) distribution, shown as the solid line in the figures. The MB fits provide an approximate temperature for the species in the beam. Also, the integrated flux of each component was determined, and this information was used to determine the composition of the beam. Cracking of O_2 into O upon ionization in the electron bombardment ionizer accounted for 11% of the O signal. Also, the ratio of the O_2 to O ionization cross sections used in these calculations was 1.9 [27]. Ultimately, the flux of O atoms that impinged on a 3-mm-diameter spot (detector viewing area) on the surface was determined for each set of operating conditions.

Table 1. Summary of Source Characterization Results

Figure Label	Operating Pressure	Power	O Temperature	O_2 Temperature	Fraction of O atoms	O-atom flux on viewed spot
	mT	W	K	K		10^{15} atoms cm^{-2} s^{-1}
A	100	50	465	490	0.30	1.1
B	75	50	475	490	0.32	0.7
C	100	30	375	400	0.20	0.7
D	75	30	340	400	0.19	0.4

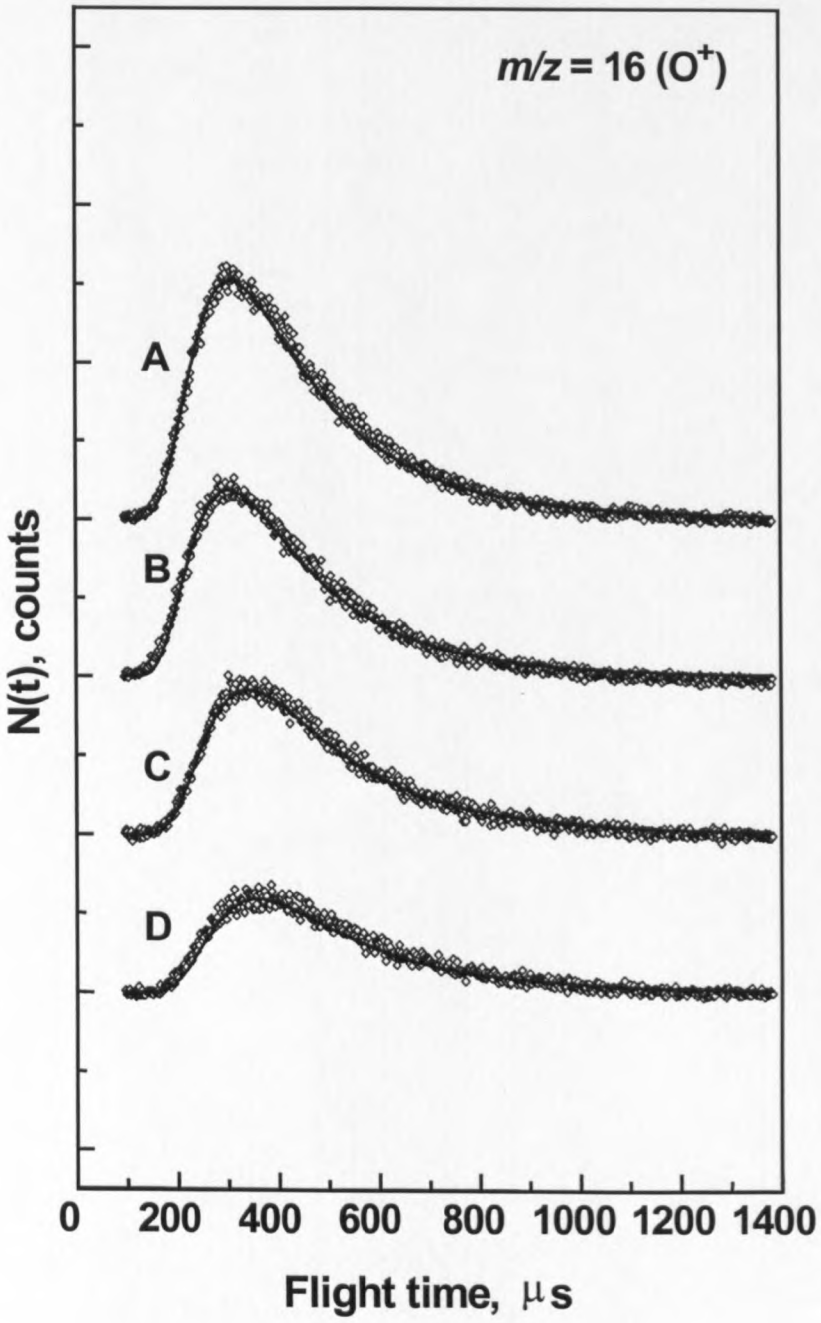

Figure 19. Time-of-flight distributions of O atoms effusing from the plasma source under four operating conditions. The labels correspond to the conditions described in Table 1. The solid curve corresponds to a Maxwell-Boltzmann distribution at the temperature listed in Table 1.

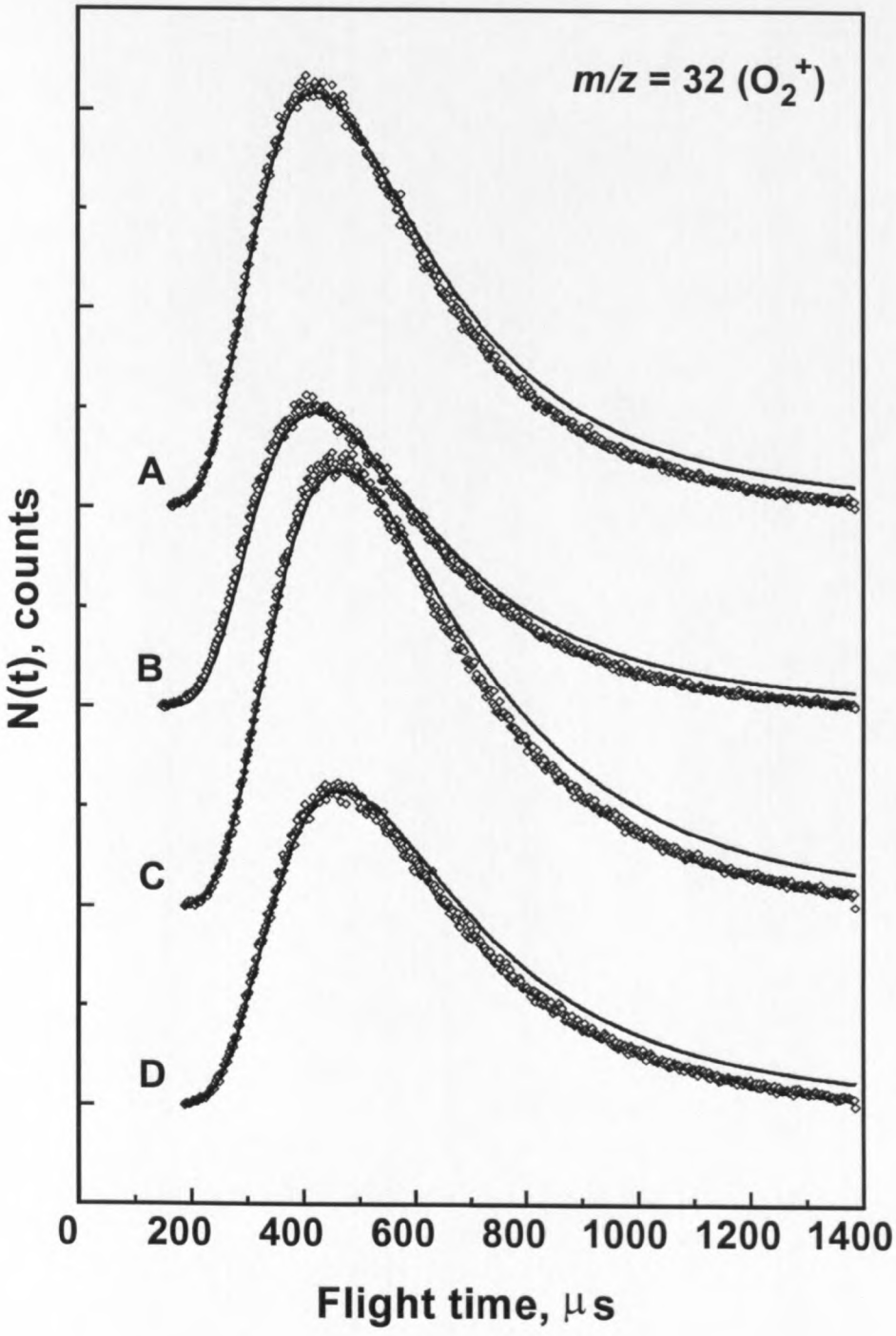

Figure 20. Time-of-flight distributions of O_2 effusing from the plasma source under four operating conditions. The labels correspond to the conditions described in Table 1. The solid curve corresponds to a Maxwell-Boltzmann distribution at the temperature listed in Table 1.

Table 1 summarizes the results and provides a key to the labeling system for Figures 19 and 20. The characteristics versus the operating conditions mentioned previously are displayed here. The MB fits for the $m/z = 16$ distributions indicate that a small fraction of the O atoms are faster than the thermal atoms derived from the MB distribution. These atoms were neglected in the analysis, but could only enhance the desired oxidation of the polymers. These calculations assumed that the O atom distributions followed a MB velocity distribution and thus left the tube orifice with a cosine distribution.

The oxygen plasma effluent was directed at a Kapton surface, which was placed on the manipulator. The TOF chopper wheel was placed between the sample and the detector aperture so that products continuously released from the surface could be modulated. A product distribution for $m/z = 44$ (CO_2^+) was collected from the Kapton surface and is shown in Figure 21. The distribution represents the CO_2 that is desorbing from the surface with a Maxwell-Boltzmann distribution of velocities that is characteristic of the surface temperature.

Summary

After the characterization study, the most desirable operating conditions were determined to be an O_2 supply pressure of 100 mT and a coupling power of 50 watts. These conditions produced a continuous beam of oxygen atoms that correspond to a temperature of 465 K and comprise 30% of the beam. The O-atom flux that would

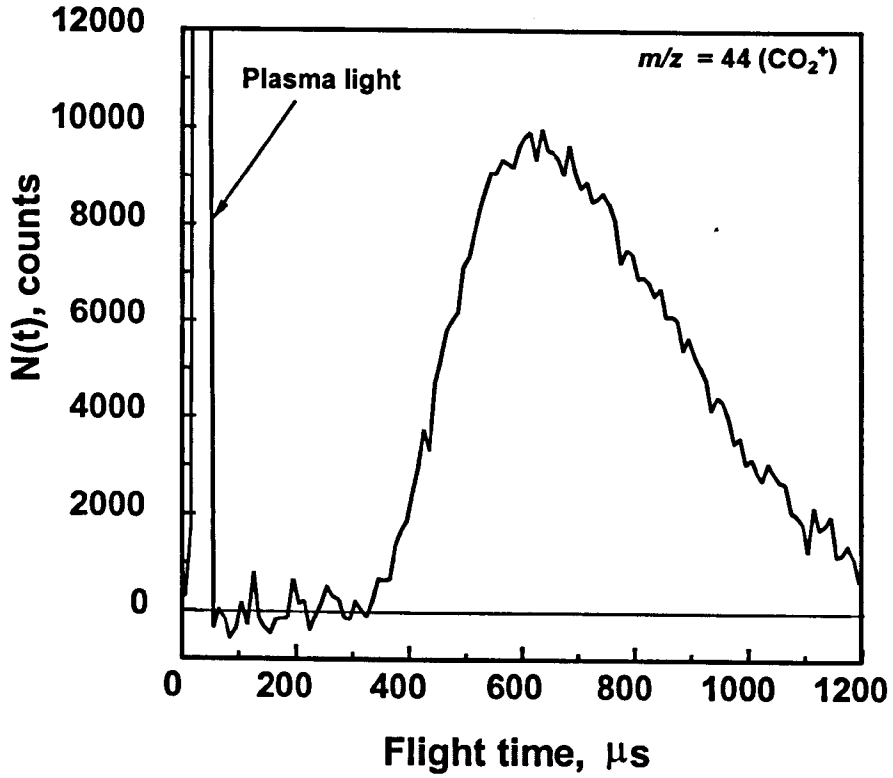

Figure 21. Time-of-flight distribution of the continuous signal of CO_2 released from the surface upon thermal oxygen atom bombardment.

impinge on the 3-mm-diameter surface spot that was 2.8 cm from the plasma tube orifice was determined to be approximately 10^{15} atoms cm^{-2} sec^{-1}. With the chopper wheel in front of the detector aperture, samples were placed on the manipulator and the plasma source was directed at the surface. A continuous thermal signal at m/z = 44 (CO_2^+) was detected from a polymer surface which was subjected to the thermal atomic oxygen. These product signals provide concrete evidence that the O atoms are oxidizing and eroding the bombarded surfaces.

CHAPTER FIVE

THE ROLE OF HYPERTHERMAL NITROGEN MOLECULES ON THE EROSION OF POLYMERS SIMULANTEOUSLY SUBJECTED TO ATOMIC OXYGEN

Introduction

The high-energy collisions (~5 eV) of atomic oxygen (AO) with spacecraft materials in low Earth orbit (LEO) frequently leads to their degradation. In particular, carbon-based materials suffer material loss in LEO, presumably because the oxides of carbon (CO and CO_2) are volatile. Testing has been conducted in space and in ground-based facilities in order to evaluate the durability of candidate materials in space [1-3, 16]. The database is now large; however, test environments differ, and disagreement persists on test standards.

A key problem in the definition of test standards is the lack of knowledge about the interactions that lead to materials degradation in space. It is generally assumed that the mechanism by which polymers erode in space involves atomic oxygen acting alone or in synergy with UV light or ions. There has been significant effort to identify the importance of synergistic effects between atomic oxygen and UV light or between atomic oxygen and ions, as these effects need to be considered in order to ensure valid interpretation of a test. Other test parameters, such as O-atom incident energy and flux, have also been considered.

However, in spite of the research that has been done, an accurate picture of the mechanism by which polymers degrade in LEO or in ground-based facilities has not been forthcoming.

The polymer erosion mechanisms are undoubtedly complex and involve initial reactions at the gas surface interface as well as material removal processes. It has been shown that CO and CO_2 are important, if not dominant, carbon-containing reaction products when a hydrocarbon polymer is subjected to the space environment or to the atomic oxygen environment in a ground-based test facility. If there is a kinetic barrier to the removal of these reaction products from the surface, then the erosion rate could be slowed. Higher surface temperatures or increased O-atom incident kinetic energies have been shown to enhance the erosion rate. Both these factors are assumed to facilitate atomic oxygen reactions; however, the observations could also be interpreted in terms of a barrier to the removal of the reaction products from the surface. If the rate of product removal from the surface is slower than the rate of formation of these products, then the material removal mechanisms, not the reaction mechanisms, could dominate the erosion yield of a polymer.

A material removal mechanism that has not been considered is collision-induced release of CO or CO_2. The LEO environment subjects materials on the "RAM" side of spacecraft to ~5 eV collisions with ambient O atoms and to ~9 eV collisions with ambient N_2 molecules. These energies are averages in distributions that have full widths at half maximum of 1.5 and 2.5 eV, respectively. In addition, an often-used source for testing in ground-based facilities, the laser-detonation source, exposes test samples to molecular oxygen with kinetic energies greater than 10 eV (i.e., roughly twice the O-atom energy). The N_2 flux in the space environment and the O_2 flux in the ground-based facility are a significant fraction

of the O-atom flux, typically 20 - 30 percent. It is possible that energetic collisions between these relatively nonreactive species and an oxidized polymer surface might promote release of volatile reaction products. Collisions between rare-gas atoms, with kinetic energies of a few eV, and halogenated silicon surfaces have been shown to promote the ejection of silicon halides from the surface [28, 29]. If such a collisional process plays a significant role to materials erosion in space, then the content of energetic neutrals in test environments should be considered and, possibly, controlled.

This chapter describes an experiment in which a beam of nitrogen molecules, with variable incident energy, was directed at continuously-oxidized polymer surfaces. Enhancement in the production of volatile CO_2 was correlated with the impinging N_2 molecules, indicating that collisions do indeed contribute to the removal of reaction products from the surface. In addition, the collisional production of CO_2 was strongly dependent on the N_2 incident energy.

Experimental Methods

This experiment was conducted with the use of a crossed molecular beams apparatus which has been described previously [19, 20]. A schematic diagram of the configuration used for this experiment is shown in Figure 22. A low-pressure RF discharge source is used to produce an effusive beam of thermal atomic oxygen. This beam impinges on a polymer surface continuously and causes it to become oxidized and slowly etched. A second, pulsed, beam of hyperthermal N_2 molecules is directed at the continuously-oxidized polymer surface.

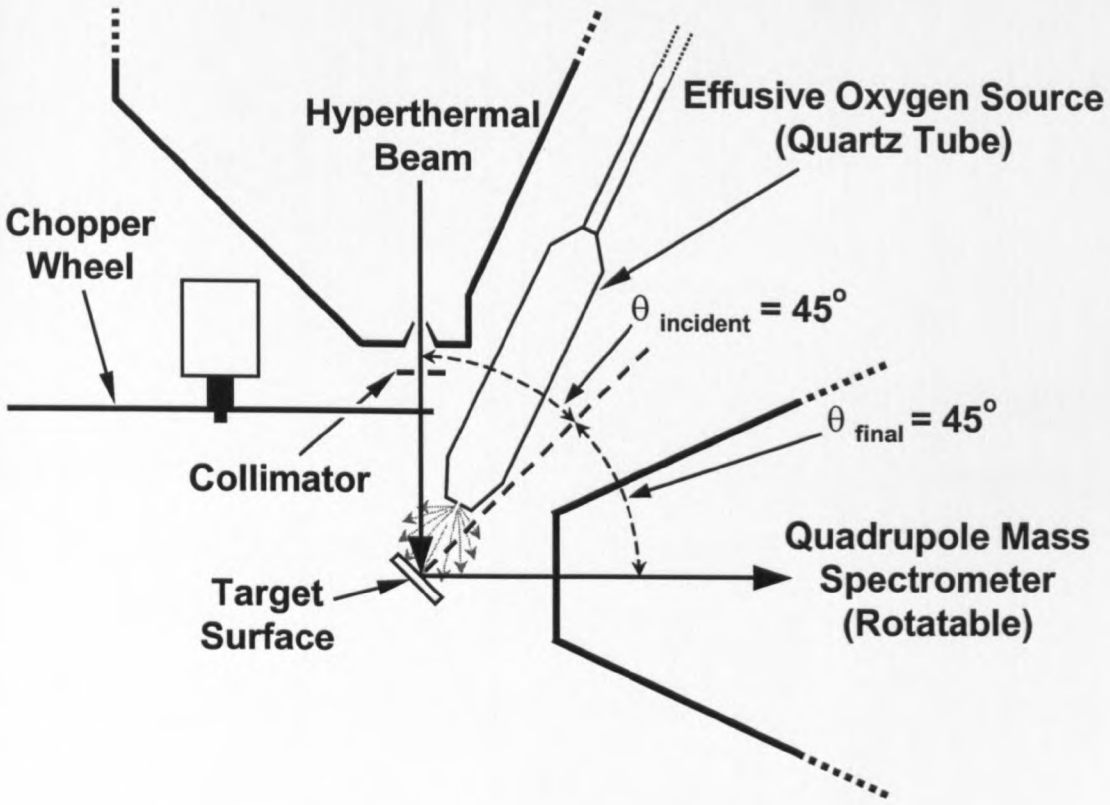

Figure 22. Schematic diagram of the interaction region of the apparatus, showing the placement of the plasma tube, chopper wheel, hyperthermal beam, and mass spectrometer detector.

The angle between the thermal and hyperthermal sources was 25°. Volatile CO_2 reaction products are monitored as a function of time after the N_2 pulse strikes the surface with the use of a rotatable mass spectrometer detector.

The sample surfaces used were Kapton polyimide and polystyrene. The Kapton surface was prepared by spin-coating the polyamic acid onto a silicon substrate and curing the film at 300°C. The film thickness was approximately 1 μm. Polystyrene samples were cut from a 0.93-mm-thick sheet obtained from Plaskolyte. The average molecular weight of the polystyrene was quoted by the manufacturer to be 100,000 g/mol. The samples were

mounted on a manipulator such that the sample surface normal was contained in the plane of the detector rotation axis. The manipulator was positioned such that its rotation axis was coincident with the detector rotation axis. The samples were thermally isolated but electrically grounded. No heating was applied to the samples other than radiative heating from the RF plasma source.

The continuous effusive atomic oxygen beam was produced by an internal inductively coupled plasma. The O_2 precursor gas was fed to a one-inch diameter quartz tube and was maintained at 0.100 Torr by a microneedle valve outside the vacuum chamber. The plasma was operated at 50 watts. Plasma products exited the quartz tube through a 0.50 mm orifice and were directed at the target on the sample manipulator. The beam was characterized by aligning the detector with the quartz tube orifice and placing a chopper wheel before the detector to modulate the beam. The energy distribution of the effusive beam could be approximately fit by a Maxwell-Boltzmann distribution and corresponded to temperatures of 465 K and 485 K for the O and O_2 components, respectively. The fraction of O atoms in the beam was 30 %, and with the orifice a distance of 2.8 cm from the target surface, the flux of O atoms on the surface was approximately 10^{15} atoms cm^{-1} sec^{-1}. With the electron impact ionizer turned off, the number of ions in the O/O_2 beam was undetectable (within the noise of the detector). Thus, the plasma source provided a continuous neutral beam of only atomic and molecular oxygen.

The hyperthermal source was the laser-detonation source that has been described earlier [21]. Both O_2 and N_2 were used as feed gases, resulting in the production of pulsed neutral beams containing O and O_2 in a molar ratio of approximately 50:50 or N and N_2 in a

molar ratio of approximately 20:80, respectively. The beam pulses effectively originated from a point source and had fairly broad energy distributions. The beam pulses passed out of the differentially-pumped source chamber through a 3-mm-diameter skimmer and were chopped by a velocity-selecting chopper wheel. The chopper wheel was a slotted disk that was synchronized with the beam pulse.

Time-of-flight distributions of incident beams were collected with the mass spectrometer detector and allowed the determination of the energy distributions of the atoms and molecules in the beams. By changing the synchronization of the chopper, four different O/O_2 beams were created, with energy distributions shown in Figure 23, and these beams were directed at an oxidized polystyrene surface. Likewise, four different N/N_2 beams were created and directed at an oxidized polystyrene surface. An additional experiment was conducted in which three different N/N_2 beams were directed at an oxidized Kapton surface. Normalized energy distributions of the N_2 beams are shown in Figure 24.

Product time-of-flight (TOF) distributions were collected at a mass-to-charge ratio (*m/z*) of 44, corresponding to CO_2^+. The TOF signals were averaged for 2,000 pulses of the hyperthermal O/O_2 beams and for 3,000 pulses (polystyrene) or 4,500 pulses (Kapton) of the N/N_2 beams. For the experiments described here, the incident angle of the hyperthermal beams and the detection angle were both 45° with respect to the surface normal.

Results and Analysis

The continuous beam of thermal atomic and molecular oxygen from the plasma source oxidized and eroded the polymer surface. Evidence for the reaction of this effusive

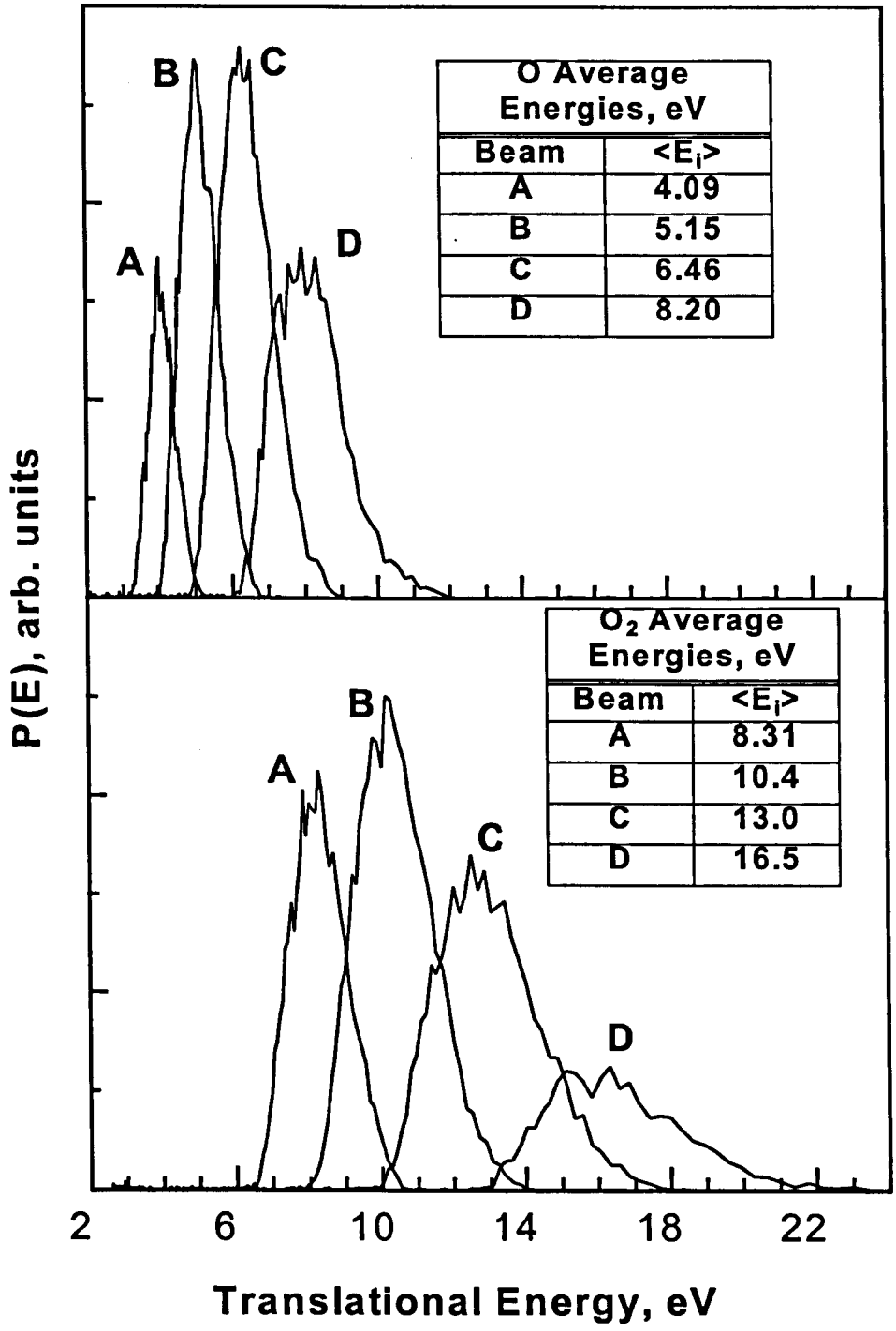

Figure 23. Translational energy distributions of the O and O_2 components for the different beams. The O_2 beams have been normalized to reflect the respective intensities of the O_2 beams. The O beams have been normalized to represent the ratio of O to O_2 in each beam.

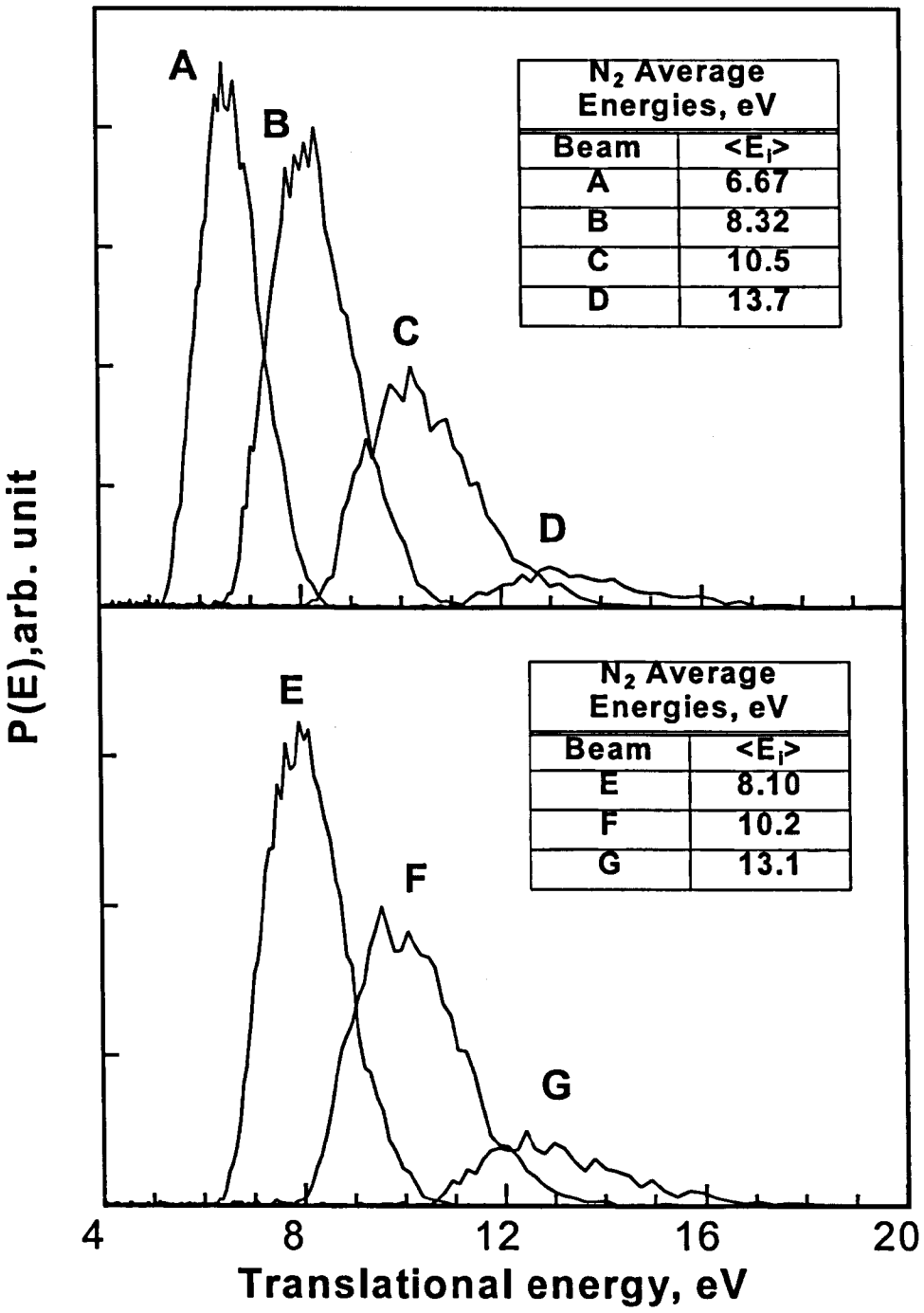

Figure 24. Translational energy distributions of the N_2 component from N/N_2 beams. The top panel shows the beams which struck the polystyrene surface, and the bottom panel shows the beams which struck the Kapton surface. The beams are normalized to the other beams in the respective panels.

beam with the sample surfaces was seen in the detection of CO and CO_2 reaction products from the surfaces that were exposed to this beam and in the observed erosion of the sample after long-term exposure. TOF distributions of the CO and CO_2 products were monitored by placing a chopper wheel between the surface and detector. The shape of these distributions typically became constant within one hour of exposure, indicating that steady-state conditions had been reached. All data reported here were collected under steady-state erosion conditions. We found that a Kapton surface eroded about 1 μm after 16 hours of exposure. As the surface is eroded, it becomes increasingly roughened. We endeavored to collect all data with fresh samples that were exposed to the effusive source for only a few hours, in order to minimize the effect of surface roughening on the data. We verified the negligible effect of surface roughening by checking the reproducibility of product TOF signals throughout the experiments.

TOF distributions collected at $m/z = 44$ (CO_2^+) that were produced from the collision of the pulsed hyperthermal O/O_2 beams with the continuously-oxidized polystyrene surface are shown in Figure 25. The production of CO_2 from exposure to the effusive beam created a continuous background that was subtracted. The distributions in Figure 25 are labeled with letters that relate each product TOF distribution to its corresponding incident beam distribution (Figure 23). The product TOF distributions were normalized to the integrated intensities of the O_2 component in the respective incident beams. Time zero in the TOF distributions corresponds to the time at which the maximum intensity of the O_2 component in the incident beam struck the surface.

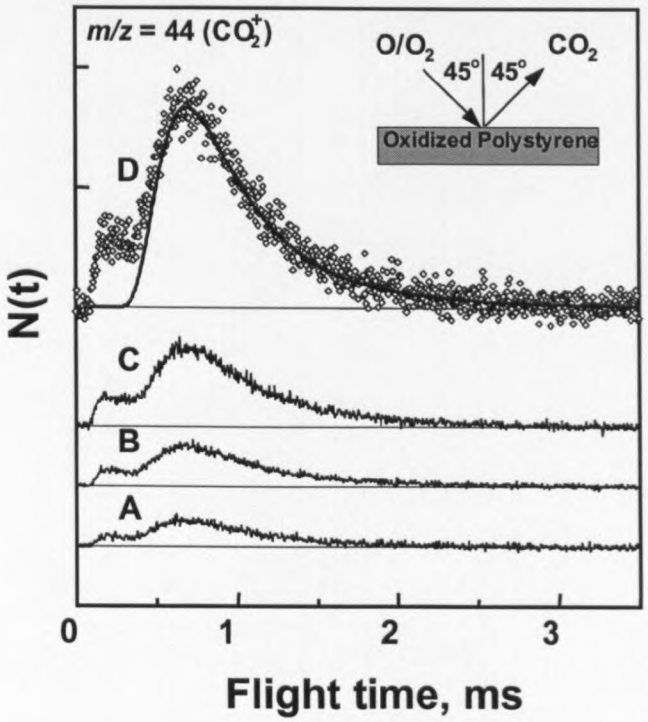

Figure 25. Time-of-flight distributions of CO_2 produced from four O/O_2 beams with corresponding energies shown in Fig. 23. Curve D shows a Maxwell-Boltzmann fit to the slow component.

The TOF distributions of the CO_2 product are bimodal, indicating two distinct mechanisms through which CO_2 leaves the surface following impact of the hyperthermal beam. We separated the two components by assuming that the slower component corresponded to CO_2 molecules which exited the surface with a Maxwell-Boltzmann (MB) distribution of velocities corresponding to the surface temperature. An example of the MB fit to the slow component is shown for curve D in Figure 25. Subtraction of the MB component from the overall TOF leaves the hyperthermal component, corresponding to CO_2 molecules which exited the surface with energies much greater than thermal energies at the

surface temperature. We found that the average energies of the hyperthermal components were approximately the same (~0.7 eV) regardless of the incident energy.

The top panel in Figure 26 shows the TOF distributions of $m/z = 44$ (CO_2^+) produced by different incident beams of N_2, whose corresponding energies are shown in the top panel of Figure 24. The product signals were normalized to the integrated intensities of the N_2 components in the respective incident beams. The lowest N_2 beam energy of 6.67 eV did not produce any detectable CO_2. As the incident beam energy increased up to 13.7 eV, the intensity of the CO_2 product dramatically increased, and this increase is shown in the bottom panel of Figure 26, where the total integrated intensity is plotted as a function of the incident energy. Although total intensity is plotted here, a plot of the intensity of either the hyperthermal or thermal component as a function of energy looks about the same, because the intensities of these components increase at the same rate with incident energy.

The N_2 beams, whose translational energy distributions are shown in the bottom panel of Figure 24, were directed at a Kapton surface, and the corresponding TOF distributions of $m/z = 44$ (CO_2^+) are shown in the top panel of Figure 27. These distributions were also normalized with respect to the intensity of the respective incident N_2 beams. Again, the integrated intensity of the CO_2 product signal increases exponentially with increasing incident energy (bottom panel, Figure 27).

Similar to the product distribution from the O/O_2 beam, collisions of energetic N_2 with the surface also produce bimodal TOF distributions of CO_2, and this behavior is observed whether the sample was oxidized polystyrene or Kapton. The deconvolution of the overall signal with the 13.1 eV N_2 beam on the oxidized Kapton surface is shown in Figure 28.

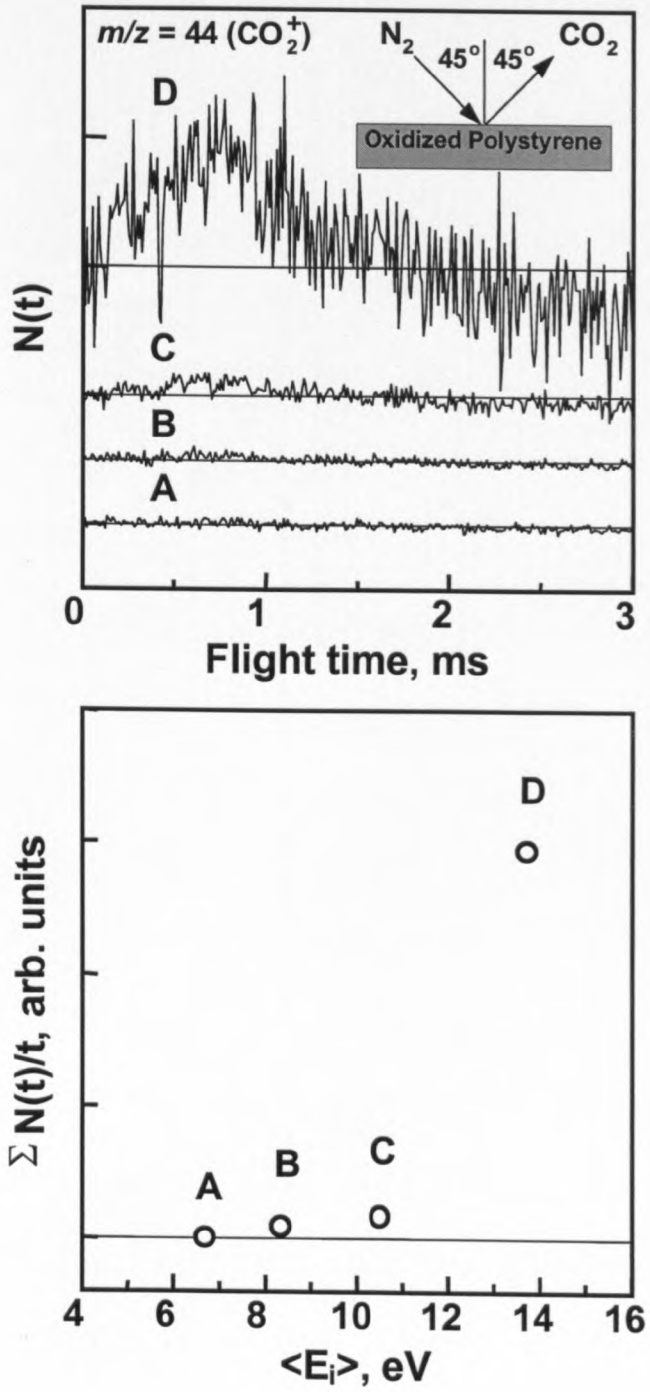

Figure 26. Results of hyperthermal N_2 incident on oxidized polystyrene. The top panel shows the TOF distributions of CO_2 released from the surface upon impact of the four beams whose conditions are shown in the top panel of Fig. 24. The distributions are normalized with respect to the incident beam intensity. The bottom panel shows the total integrated intensity as a function of incident beam energy.

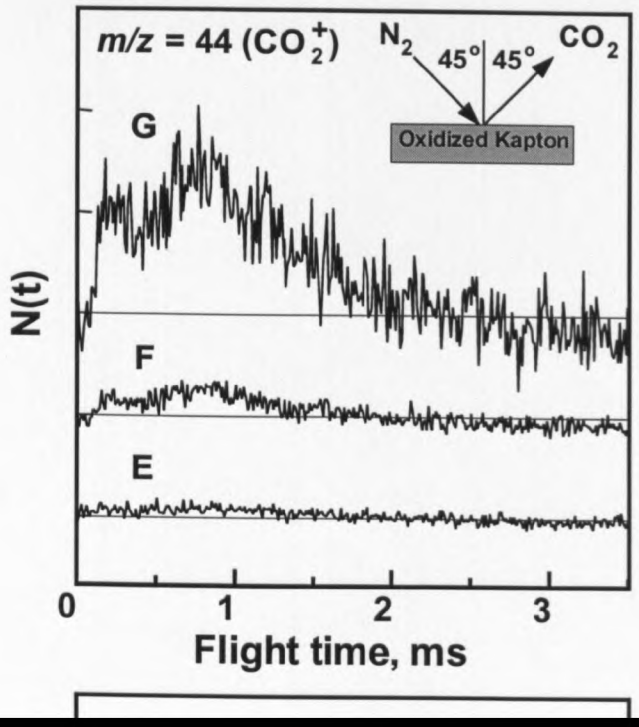
m/z = 44 (CO_2^+)
N_2
45°
45°
CO_2
Oxidized Kapton
G
F
E
N(t)
0
1
2
3
Flight time, ms